

77 270

IDENTIFICATION OF NOISE SOURCE IN WHEELCHAIR

**A Thesis Submitted to the
Graduate School of Natural and Applied Sciences of
Dokuz Eylül University
In Partial Fulfillment of the Requirements for
the Degree of Master of Science in Electrical and Electronics
Engineering**

by

Osman GERGÖZ

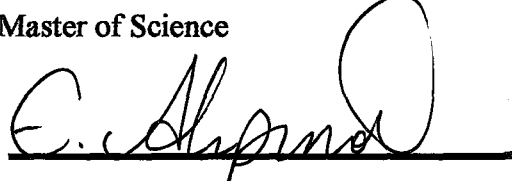
77270

September, 1998

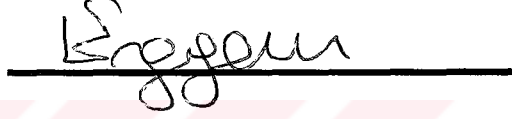
İZMİR

THESIS EXAMINATION RESULT FORM

We certify that we have read this thesis and that in our opinion it is fully adequate, in scope and in quality, as a thesis for the degree of Master of Science



Assoc. Prof. Dr. Eyüp AKPINAR
(Advisor)

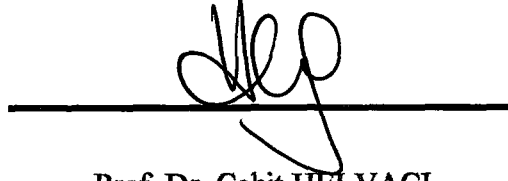


(Committee Member)



(Committee Member)

Approved by the
Graduate School of Natural and Applied Sciences



Prof. Dr. Cahit HELVACI
Director

ACKNOWLEDGEMENTS

I wish to express my gratitude to my advisor, Assoc. Prof. Dr. Eyüp AKPINAR for his sincerely guidance during this study of thesis and FAZ ELEKTRİK motor company which is my firm for their financial and technical supports.

Osman GERGÖZ

ABSTRACT

The identification of noise sources in a wheelchair which is powered by electric motors and designed for disabled person who have lost their mobility is presented in this thesis. The permanent magnet direct current motors used in wheelchair have been considered as the main source of audible noise and vibration in a wheelchair. First the operating point of the motor has been determined using magnetic field analysis then the electromagnetic radial force that causes the noise and the vibration in an electric motor has been analysed. The frequency spectrum of the vibration signal has been obtained by a vibrometer device has been obtained. Additionally, the frequency spectrum of the noise signal acquired with a general purpose microphone has been given. A relation between the frequency spectrum of the electromagnetic radial forces computed in MATHLAB and measurement of vibration and noise using Data Acquisition System (DAS) are given in this study.

ÖZET

Bu tezde, hareket yeteneğini kısmen ya da tamamen kaybetmiş özürlü kimseler için tasarlanmış elektrik motorlu özürlü sandalyesinden yayılan duyulabilir gürültü kaynaklarının ne vibrasyonun tanımlanması yapılmıştır. Özürlü sandalyesindeki vibrasyon ve gürültü kaynağı olarak, kullanılan sabit mıknatıslı doğru akım motoru düşünülmüştür. Öncelikle motorun çalışma noktası magnetic alan analizi ile tanımlanmış, daha sonra gürültü ve vibrasyona sebep olan elektromagnetik radyal güçler analiz edilmiştir. Bir vibrometre aracılığı ile toplanan vibrasyon sinyalinin frekans spektrumu elde edilmiştir. Buna ek olarak genel kullanım amaçlı bir mikrofon yardımı ile elde edilen gürültü sinyalinin de frekans spektrumu verilmiştir. MATHLAB’da hesaplanan electromagnetic radyal güçlerin frekans spektrumu ile Veri Toplama Sistemi (VTS) aracılığıyla fiziksel olarak ölçülen gürültü ve vibrasyon sinyallerinin frekans spektrumları karşılaştırılmış ve aralarındaki ilinti verilmiştir.

CONTENTS

	Page
Contents	VII
List of Figures.....	III
List of Tables.....	IV

Chapter One INTRODUCTION

1. INTRODUCTION.....	1
----------------------	---

Chapter Two ELECTROMAGNETIC RADIAL FORCES

2. ELECTROMAGNETIC RADIAL FORCES.....	4
2.1 MMF PRODUCED BY THE MAGNETS	4
2.1.1 MODIFIED MAGNETIC CIRCUIT APPROACH	5
2.1.1.1 DEMAGNETISATION CURVE OF MAGNET	5
2.1.1.2 MAGNETISATION CHARACTERISTIC OF STEEL.....	6
2.1.1.3 EQUIVALENT MAGNETIC CIRCUIT OF MOTOR	8
2.1.1.4 MODIFIED F - Φ CURVES	9
2.1.1.5 OBTAINING OH THE CURVES	10
2.2 SEARCH COIL VOLTAGE	15

2.3 PERMEANCE OF THE MOTOR	18
2.4 FLUX DISTRIBUTION IN THE AIR GAP	21
2.5 FLUX DENSITY DISTRIBUTION IN THE AIR GAP	22
2.6 ELECTROMAGNETIC RADIAL FORCES	24

Chapter Three

NOISE AND VIBRATION

3 NOISE AND VIBRATION	32
3.1 SOUND WAVES	
32	
3.2 THE NOISE AND THE VIBRATION SOURCE IN WHEELCHAIR MOTOR	33
3.2.1 COMMUTATOR END COVER	34
3.2.2 BODY YOKE AND ARMATURE	34
3.2.3 GEAR	36
3.3 MEASURING DEVICES	37
3.3.1 SENSORS	38
3.3.1.1 NOISE SENSOR	39
3.3.1.2 VIBRATION SENSOR	39
3.3.2 PREAMPLIFIER	39
3.3.3 PERSONAL COMPUTER	40
3.3.4 DATA ACQUISITION SYSTEM	40
3.3.4.1 DATA ACQUISITION HARDWARE	40
3.3.4.2 DATA ACQUISITION SOFTWARE	40

Chapter Four
RESULTS AND CONCLUSIONS

4. RESULTS AND CONCLUSIONS	42
4.1 THE EXPERIMENTAL RESULTS	42
4.1.1 THE FFT OF THE VIBRATION OF WHEELCHAIR	42
4.1.2 THE FFT OF THE VIBRATION OF THE MOTOR COUPLED WITH A GEAR SYSTEM	45
4.1.3 THE FFT OF THE VIBRATION OF THE MOTOR WITHOUT A GEAR SYSTEM	47
4.1.4 THE FFT OF THE NOISE AND THE VIBRATION OF THE MOTOR ROTATED BY AN EXTERNAL PRIME MOVER	47
4.2 THE THEORETICAL RESULTS	51
4.3 COMPARISON BETWEEN EXPERIMENTAL AND THEORETICAL RESULTS	53
4.4 CONCLUSIONS	53
REFERENCES	54
APPENDIX	56

LIST OF FIGURES

	Page
Figure 2.1 Demagnetisation curve of a magnet	5
Figure 2.2 The magnetisation characteristic of steel used in lamination and core	6
Figure 2.3 The Per pole magnetic equivalent circuit of motor	8
Figure 2.4 The modified $F-\Phi$ curves in a motor	9
Figure 2.5 (a) Search coil insertion and flux distribution, (b) average flux in search coil with respect to rotor position, (c) induced emf in search coil ..	16
Figure 2.6 Experimentally obtained search coil voltage on an oscilloscope screen	18
Figure 2.7 Lay out flat view of the motor, permeance waves, MMF waves, Flux waves, flux density waves and electromagnetic radial forces waves ...	19
Figure 2.8 An enlarged section of the motor that shows slots and current carrying conductors	20
Figure 2.9 The magnetic flux path thorough the air gap and the armature laminations	21
Figure 2.10 Two different regions separated by a boundary	25
Figure 2.11 Air gap flux density	30
Figure 2.12 Electromagnetic radial forces	31
Figure 3.1 Frequency range of longitudinal mechanical waves	33
Figure 3.2 Electric motors used in the wheelchair.....	33
Figure 3.3 Body yoke and magnets	35
Figure 3.4 Armature	35
Figure 3.5 A section view of the motor	36
Figure 3.6 Configuration of data acquisition system	37
Figure 3.7 A photograph showing the measuring device.....	38

Figure 4.1 A photo of an electrically powered wheelchair and the name of its parts	43
Figure 4.2 The frequency spectrum of the vibration produced in wheelchair	44
Figure 4.3 The frequency spectrum of the vibration produced in the motor coupled with the gear system	46
Figure 4.4 The frequency spectrum of the vibration produced in the motor without the gear system	48
Figure 4.5 The frequency spectrum of the noise radiated from the motor rotated by an external prime mover	49
Figure 4.6 The frequency spectrum of the vibration produced in the motor rotated by an external prime mover	50
Figure 4.7 FFT of the electromagnetic radial forces.....	52



LIST OF TABLES

	Page
Table 1 Design data of wheelchair motor	10
Table 2 Seven point on the modified $B-H$ curve of steel	12
Table 3 The elements of regression matrixes	12
Table 4 Calculated equations	14
Table 5 The parameter of test motor	51

CHAPTER ONE

INTRODUCTION

Many companies have been trying to design and develop a lot of tools for disabled persons who have lost their mobility. One of these tools is wheelchair. There are two types of wheelchair. One is manually operated other is powered by electric motors. In the first type, disabled person or his/her guard drives wheelchair by the force applied to the back or directly to the wheels of wheelchair. However, in the other type the force required for movement is produced by the electric motors. The permanent magnet direct current motors are extensively used in all wheelchairs because of easy to drive. Generally, electronic controller governing all movement controls one pair of dc motors coupled to the rear wheels via fixed gear. A set of batteries is used as an energy source.

In order to get an optimum quality and a safely use of wheelchairs, they have to be designed and manufactured according to national or international relevant standards. First of all wheelchairs are classified within three classes in standards according to the purpose of using and then overall dimensions, excepted abilities such as maximum grading, speed, breaking distance etc. and test methods for each class are determined for utmost safe and quality (EUREPEAN NORM, TECHNICAL COMMITTEE, Pr. EN 12184, 1992).

One of these standards explains the level of audible noise radiated from wheelchair and its measuring devices. The noise level that is the measure of quality of wheelchair has to be kept under 65 dB in class A and 75 dB in class B and C.

The study to determine the noise sources in wheelchair concludes that the main source in system is the electric motors. So the aim of this thesis is specified to study the noise generated from the motors.

Many investigators have dealt with the reason of audible noise in electric motors especially in induction motors. They have considered that there is a good relation between the noise and the electromagnetic radial forces in air gap. They have verified that the electromagnetic radial forces have a pulsation wave derived from air gap flux density and this causes noise and vibration in electric motors.

Some investigators have analysed the effect of slot combination on acoustic noise. First, they have calculated the frequency spectrum of radial forces and then compared it to the noise spectrum. They have tried to find a relation between the number of the stator slots, the rotor slots and noise. (KOBAYASHI, T., & TAJIMA, F., & ITO, M., & SHIBUKAWA, S., 1997)

Similarly, the effect of the electromagnetic radial forces on noise and vibration has been analysed depending on the permeance-wave method that explains how the fluctuating magnetic flux produces these forces. (VERNA, S. P., & BALAN, A., 1994)

In order to identify the noise sources in the wheelchair, the analysis of permanent magnet motor that is used has to be studied. A modified magnetic circuit method has been applied for the analysis of direct current permanent magnet motors with differing armature, magnet and yoke lengths including non-linear material behaviour of steel and permanent magnet. (NARAYANAN, S., S., Y., & NAIR, K., R., A., 1998)

For the determination of the operating point of the motor an equivalent magnetic circuit is used. In this circuit air gap reluctance, lamination reluctance and yoke reluctance are presented. (WING, M., & GIERAS, J., F., 1992)

The electromagnetic radial and tangential forces are physically analysed at the boundary conditions (BINNS, K., J., &LAWRENSON, P., J., &TROWBRIDGE, C., W., 1995).

With the guidance of the works mentioned above the study on the noise and the vibration produced in wheelchair is carried out in this thesis. In Chapter II, a technique for determining the operating point of the motor is developed. For that the MMF produced by the magnets is defined and this technique is verified by the comparison with the search coil voltage. Then the electromagnetic radial forces are computed. For that the permeance waves, flux and flux density distribution in the air gap are individually presented. Finally, Fourier Series of the electromagnetic radial forces is obtained.

In Chapter III, the noise and the vibration are related to the magnetic field. The noise and the vibration produced in the different part of the motor are studied. Also, the measuring devices used in the experimental set up are introduced in this Chapter.

In Chapter IV the experimental results are presented for complete wheelchair, motor with and without gear assembly and rotated by an external-moving device. The theoretical results computed in MATHLAB are compared with the actual measurements. Finally, the conclusion and further works are given in the last Chapter.

CHAPTER TWO

ELECTROMAGNETIC RADIAL FORCES

In this chapter electromagnetic radial forces, that are the main source of noise and vibration of a motor, have been analytically expressed. The permeance waves are formulated by incorporating the effects of slotting and the magneto motive force (MMF) produced by the magnets is determined. The magnetic flux is found by the multiplication of the MMF and the permeance waves. The electromagnetic radial forces, known as Maxwell's forces, that are proportional to the square of the flux density are finally expressed.

In order to express the MMF produced by the magnets a technique is developed. In this technique a modified circuit method are presented for the analysis of d.c. permanent magnet motor with differing armature, magnet and yoke lengths including non-linear material behaviour of steel and permanent magnet.

For the verification of the calculations the analytically determined search coil voltage is compared with the experimental values.

2.1 MMF PRODUCED BY THE MAGNETS

For the determination of the operating point of the motor a modified circuit approach is applied. In this approach the demagnetisation curve of magnet and magnetisation curve of steel used in lamination and yoke are modified. Then the MMF produced by magnets is found out using the equivalent magnetic circuit of the motor.

2.1.1 MODIFIED MAGNETIC CIRCUIT APPROACH

MMF required to drive a specified value of flux through the magnetic paths of motor namely yoke, air gap and armature lamination core can be determined from the B - H characteristics of respective material. The MMF required line can be drawn by considering various flux values and calculating corresponding MMF needed to drive the flux through all magnetic paths.

2.1.1.1 DEMAGNETISATION CURVE OF MAGNET

Demagnetisation curves of a magnet is given in Figure 2.1.

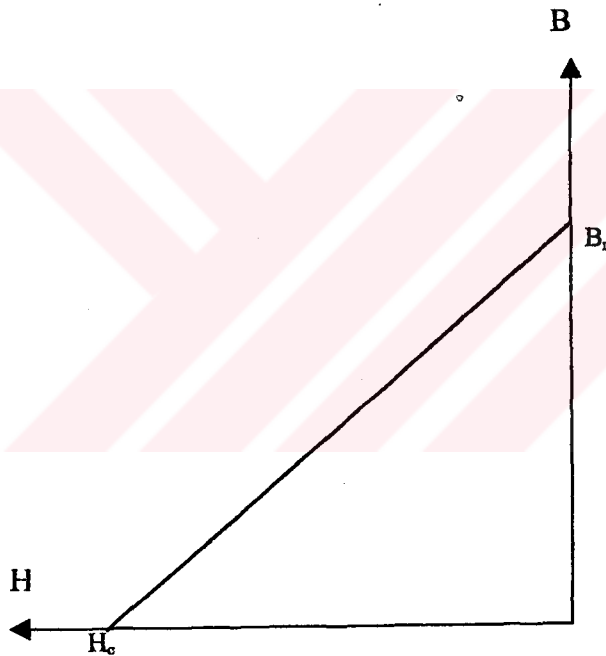


Figure 2.1. Demagnetisation curve of a magnet.

The demagnetisation curve of the magnet is expressed as follows;

$$H(B)_m = \frac{H_c}{B_r} B - H_c \quad (2.1)$$

Effect of magnet overhang is treated by multiplying magnetisation (B) value of each point on two quadrant B - H characteristics for a given magnetic strength (H) through a factor K_m and treating the length of magnet same as armature. K_m is empirically given as follows (Philips Handbook on “Design of Permanent Magnet Motors”, 1995, p. 145);

$$K_m = 1 + \left[2 * \left(1 - e^{-\frac{3.4(l_{ar}-l_m)}{D_a}} \right) * \left(1 - e^{-\frac{D_a}{6l_{ar}}} \right) \right] \quad (2.2)$$

Where;

l_{ar} : Armature length,

l_m : Magnet length,

D_a : Armature outer diameter,

2.1.1.2 MAGNETISATION CHARACTERISTIC OF STEEL

The magnetisation characteristic of steel used in lamination and core is given in Figure 2.2.

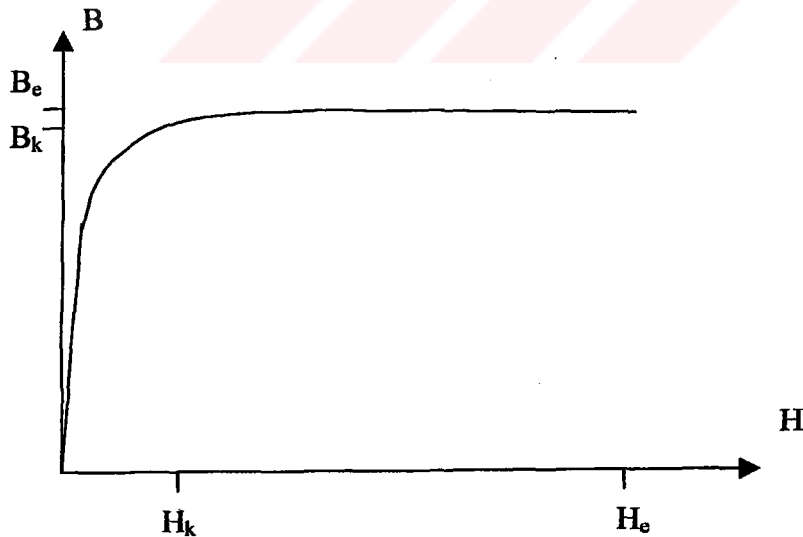


Figure 2.2. The magnetisation characteristic of steel used in lamination and core

In modified circuit approach the magnetisation characteristic of yoke's steel is modified by multiplying B by a factor equal the ratio of yoke length to armature length for each H value. The modification factor of steel symbolised K_s is expressed as follows(NARAYANAN, S., S., Y., & NAIR, K., A., & NARAYANAN, V.1998. pp. 55-61);

$$K_s = \frac{l_y}{l_{ar}} \quad (2.3)$$

Where;

l_y : Yoke length,

The magnetisation characteristic of yoke's steel can be represented by two curves one is third order the other is linear. The first curve is considered from zero to knee point (B_k, H_k) , the other is from this point to the end (B_e, H_e) . The third order curve is obtained by the regression analysis.

The n points, $(x_1, y_1), (x_2, y_2), \dots, (x_n, y_n)$, are given on B - H curve. Let the third order equation be defined as follows;

$$y = a_0 + a_1x + a_2x^2 + a_3x^3 \quad (2.4)$$

The coefficients of this equation can be obtained from matrix form;

$$\begin{bmatrix} n & \sum_{i=1}^n x_i & \sum_{i=1}^n x_i^2 & \sum_{i=1}^n x_i^3 \\ \sum_{i=1}^n x_i & \sum_{i=1}^n x_i^2 & \sum_{i=1}^n x_i^3 & \sum_{i=1}^n x_i^4 \\ \sum_{i=1}^n x_i^2 & \sum_{i=1}^n x_i^3 & \sum_{i=1}^n x_i^4 & \sum_{i=1}^n x_i^5 \\ \sum_{i=1}^n x_i^3 & \sum_{i=1}^n x_i^4 & \sum_{i=1}^n x_i^5 & \sum_{i=1}^n x_i^6 \end{bmatrix} * \begin{bmatrix} a_0 \\ a_1 \\ a_2 \\ a_3 \end{bmatrix} = \begin{bmatrix} \sum_{i=1}^n y_i \\ \sum_{i=1}^n yx_i \\ \sum_{i=1}^n yx_i^2 \\ \sum_{i=1}^n yx_i^3 \end{bmatrix} \quad (2.5)$$

In the linear region from (B_k, H_k) to (B_e, H_e) the modified magnetisation characteristic of yoke's steel is represented as follows;

$$H(B)_{s2} = \frac{H_e - H_k}{K_s(B_e - B_k)}(B - K_s B_k) + H_k \quad (2.6)$$

2.1.1.3 EQUIVALENT MAGNETIC CIRCUIT OF MOTOR

The per pole magnetic equivalent circuit of motor is shown in Figure 2.3.

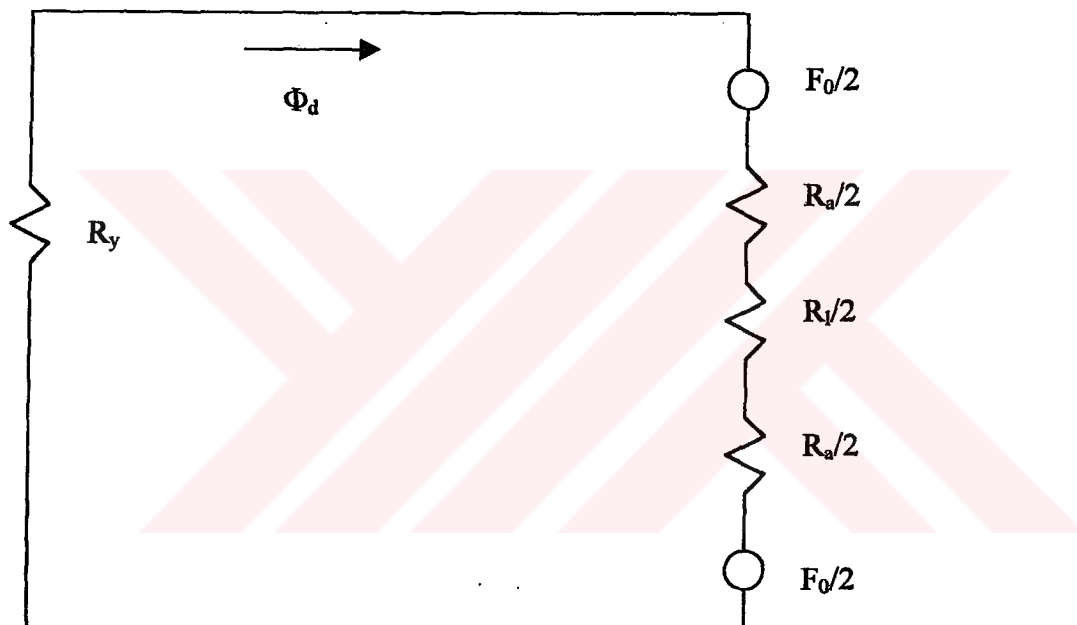


Figure 2.3. The per pole magnetic equivalent circuit of motor.

In this circuit the yoke, the lamination and the air gap reluctance are individually symbolised with R_y , R_l , R_a , respectively. This circuit represents the magnetic path per pole.

2.1.1.4 MODIFIED F - Φ CURVES

The modified F - Φ curve in a motor is plotted in Figure 2.4 by the using the following relations between H , F , B and Φ transformations.

$$H = \frac{F}{l} \quad (2.7)$$

$$B = \frac{\Phi}{S} \quad (2.8)$$

Where l and S are individually effective length and area of flux path thorough each material, respectively.

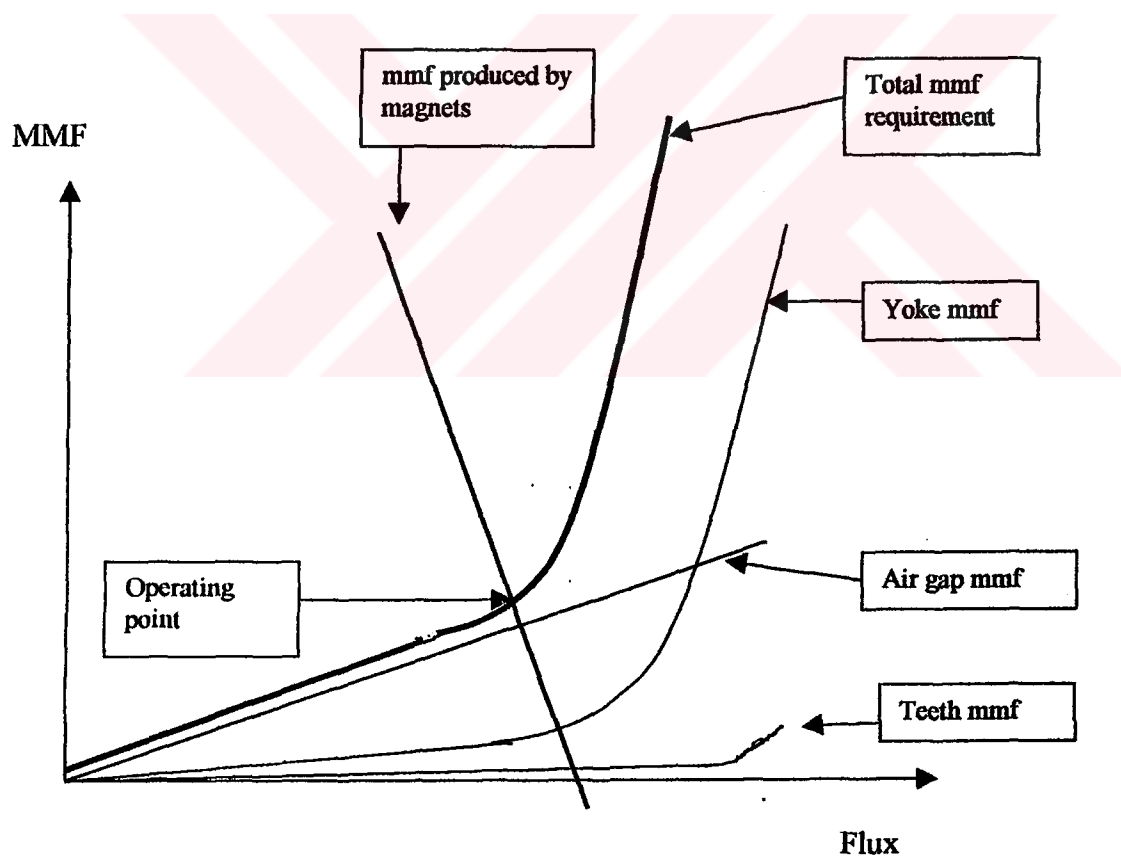


Figure 2.4. The modified F - Φ curves in a motor.

The intersection point between MMF produced by magnets and total MMF requirement provides the average operating flux per pole.

2.1.1.5 OBTAINING OF THE CURVES

To determine the operating point of wheelchair motor the machine parameters are substitute into the equations. The design data of the motor is given in Table 1.

Table 1. Design data of wheelchair motor.

Rated voltage	U	24	Volts
Rated input power	P_i	300	Watts
Yoke outer diameter	D_o	78.2	mm
Yoke inner diameter	D_i	72	mm
Yoke length	l_y	101	mm
Magnet inner diameter	D_m	58.2	mm
Magnet length	l_m	50	mm
Magnet thickness	W_m	6.9	mm
Number of poles	p	2	
Armature outer diameter	D_a	56.1	mm
Armature length	l_{ar}	50	mm
Number of slots in lamination	k	12	
Lamination slot width	W_s	3.4	mm
Lamination tooth width	W_t	11	mm
Number of turns in a coil	N	16	Turns
Coil span		1 to 7	
Central angle of magnet	α	120	degree
Residual flux density of magnet	B_r	0.392	Tesla
Coercive magnetic field strength of magnet	H_c	295	kA/m
Knee point of demagnetisation curve of steel	(B_k, H_k)	(1.63,4)	(Tesla,kA/m)
End point of demagnetisation curve of steel	(B_e, H_e)	(2,16)	(Tesla,kA/m)

Before the substituting the variables into the equations the following expressions have to be defined;

Effective length of flux path in yoke, L_y ;

$$L_y = \pi \frac{D_o + D_i}{4} \quad (2.9)$$

Effective cross sectional area in yoke, S_y ;

$$S_y = l_y \frac{D_o - D_i}{2} \quad (2.10)$$

Effective length of flux path in air gap, L_a ;

$$L_a = D_m - D_a \quad (2.11)$$

Effective cross sectional area in air gap, S_a ;

$$S_a = \frac{\alpha}{360} 2\pi \frac{D_m}{2} l_m \quad (2.12)$$

Effective length of flux path in magnets, L_m ;

$$L_m = \frac{D_i - D_m}{2} \quad (2.13)$$

Effective cross sectional area in magnets, S_m ;

$$S_m = \frac{\alpha}{360} 2\pi \frac{D_m}{2} l_m \quad (2.14)$$

It is here noted that the armature lamination MMF drop is neglected. The interpolation of B - H curve of steel in the third order region is obtained using the regression analysis as follows;

$$H(B)_{s1} = a_0 + a_1B + a_2B^2 + a_3B^3 \quad (2.15)$$

For $K_s=2.02$, seven points on the modified B - H curve of steel are given in Table 2.

Table 2. Point on the modified B - H curve of steel.

$B(\text{Tesla})$	0	1.55	1.99	2.52	2.86	3.15	3.29
$H(\text{KA/m})$	0	0.25	0.5	1	2	3	4

The elements of matrix in equation (2.5) are given in Table 3.

Table 3. The elements of regression matrixes.

n	$\sum B$	$\sum B^2$	$\sum B^3$	$\sum B^4$	$\sum B^5$	$\sum B^6$	$\sum H$	$\sum HB$	$\sum HB^2$	$\sum HB^3$
7	15.36	41.639	117.87	344.31	1028.7	3124.4	10.75	32.2325	98.3542	303.874

If these values are substituted into the matrix, the coefficients of (2.15) are obtained as follows;

$$a_0=0.0051 ; a_1=1.4217 ; a_2=-1.4472 ; a_3=0.4169$$

The modified F - Φ curve of yoke's steel is obtained below;

$$F_{y1} = \left\{ \left(a_0 L_y + a_1 \frac{L_y}{S_y} \Phi + a_2 \frac{L_y}{S_y^2} \Phi^2 + a_3 \frac{L_y}{S_y^3} \Phi^3 \right) * 10^3 \right\}; \text{ for the third order region (2.16)}$$

$$F_{y2} = L_y \frac{H_e - H_k}{K_s (B_e - B_k)} \left(\frac{1}{S_y} \Phi - K_s B_k \right) + L_y H_k ; \text{ for linear region (2.17)}$$

The modified F - Φ curve of air gap is;

$$F_a = \frac{L_a}{\mu_0 S_a} \Phi \quad (2.18)$$

Total F - Φ curve of motor is;

$$F_{req1} = F_{y1} + F_a; \text{ for the third order region (2.19)}$$

$$F_{req2} = F_{y2} + F_a; \text{ for the linear region (2.20)}$$

The modified F - Φ curve of magnet is;

$$F_m = \frac{H_c}{K_m B_r} \frac{L_m}{S_m} \Phi - L_m H_c \quad (2.21)$$

The equations using the parameters of the motor are given in Table 4.

Table 4. Calculated equations

Symbol	Reference equation	Calculated equation or value
$H(B)_m$	2.1	$(0.753B-0.295)*10^6$
K_m	2.2	1
K_s	2.3	2.02
L_y	2.9	$117.97*10^{-3} \text{ mm}$
S_y	2.10	$313.1*10^{-6} \text{ mm}^2$
L_a	2.11	$2.01*10^{-3} \text{ mm}$
S_a	2.12	$3047*10^{-6} \text{ mm}^2$
L_m	2.13	$6.9*10^{-3} \text{ mm}$
S_m	2.14	$3047*10^{-6} \text{ mm}^2$
$H(B)_{s1}$	2.15	$(0.0051+1.4217B-1.4472B^2+0.4169B^3)10^3 ; 0<B<4 \text{ Tesla}$
$H(B)_{s2}$	2.6	$(16B-48.86)10^3 ; 4<B<16 \text{ Tesla}$
$F(\Phi)_{y1}$	2.16	$(0.006+535.625\Phi-1.741*10^6 \Phi^2+1.602*10^9 \Phi^3)10^3$
$F(\Phi)_{y2}$	2.17	$(-5.765+6049.1\Phi)10^3$
$F(\Phi)_a$	2.18	$525*10^3 \Phi$
$F(\Phi)_{req1}$	2.19	$(0.006+1060.625\Phi-1.741*10^6 \Phi^2+1.602*10^9 \Phi^3)10^3$
$F(\Phi)_{req2}$	2.20	$(-5.765+6574.1\Phi)10^3$
$F(\Phi)_m$	2.21	$(2.035-1704\Phi)10^3$

The operating point of motor is determined at the intersection point of total MMF and MMF produced by magnet. These two curves intersect in the third order region and this point is expressed as follows;

$$F_{req1} = F_m \quad (2.22)$$

$$(0.006+1060.625\Phi-1.741*10^6 \Phi^2+1.602*10^9 \Phi^3)10^3 = (2.035-1704\Phi)10^3 \quad (2.23)$$

Thus, the operating point, (Φ_0, F_0) is $(82.81*10^{-5} \text{ Weber}, 599.99 \text{ Amper.turn})$

2.2. SEARCH COIL VOLTAGE

For the validation of the calculations the search coil voltage is analytically obtained and plotted with respect to angular position of rotor, θ then compared with the experimentally obtained value.

The search coil is wound into 1 and 7 slots (180 degree electrical) with the same number of turns of the armature coils (16 turns). The end points of the coil have been individually soldered to the carbon brushes to maintain the wave shape of the induced voltage on an oscilloscope screen. The rotor has been rotated at 3676 rpm (61.27 Hz) by the prime mover device. The search coil insertion, mean flux and search coil voltage are shown in Figure 2.5.

The search coil rotates with the same rotational speed of the rotor. The amplitude and the shape of the flux depend on the MMF produced by the magnets. Therefore, the mean flux distribution that is the mean value of the flux wave with respect to the angular position of the rotor can be calculated and plotted for each degree. Thus, both the amplitude and the frequency of the induced voltage across the search coil that can be obtained by the derivation of the mean flux value depend on the rotational speed of the motor.

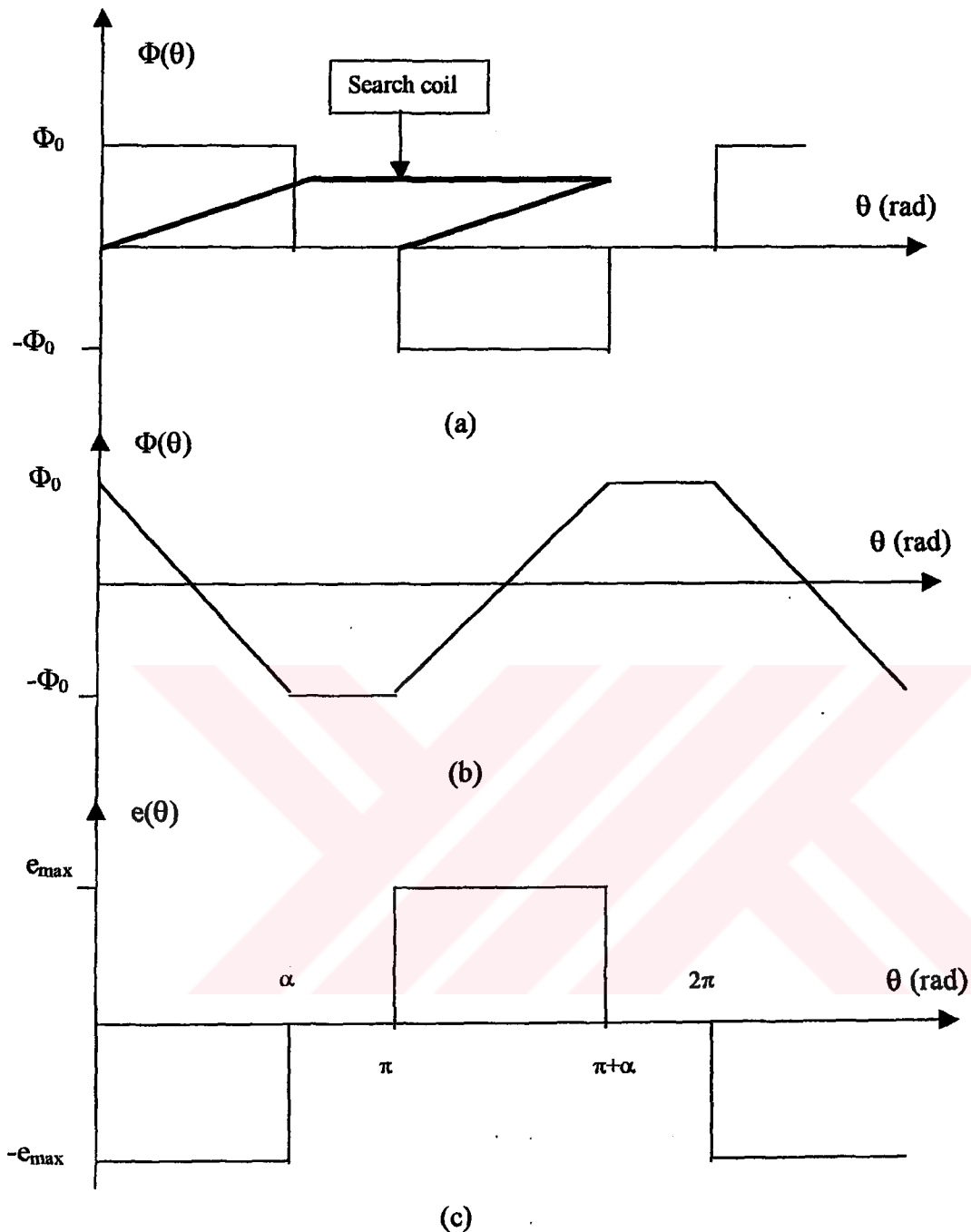


Figure 2.5. (a) Search coil insertion and flux distribution, (b) average flux in search coil with respect to rotor position, (c) induced emf in search coil.

The search coil voltage can be calculated as follows;

The amplitude of the average flux is;

$$\bar{\Phi}_0 = \alpha \Phi_0 \quad (2.24)$$

The flux linkage expression is;

$$\lambda(\theta) = N \bar{\Phi}(\theta) \quad (2.25)$$

The search coil voltage is;

$$e(\theta) = -\frac{d\lambda(\theta)}{dt} = -\frac{d\lambda(\theta)}{d\theta} \frac{d\theta}{dt} = -\omega \frac{d\lambda(\theta)}{d(\theta)} = -\omega N \frac{d\bar{\Phi}(\theta)}{d(\theta)} \quad (2.26)$$

The amplitude of the search coil voltage is;

$$e_{\max} = \omega N \frac{2\bar{\Phi}_0}{\alpha} \quad (2.27)$$

Where $\omega = 2\pi f$, f is the rotational speed in Hz.

If the actual values are substituted in (2.27) the amplitude of the search coil voltage is found out as 9.9 Volts.

The search coil voltage waveform has been experimentally obtained on the oscilloscope screen. A photograph that shows this waveform is given in Figure 2.6 where the time/div is at 5ms, Volt/div at 2 Volts.

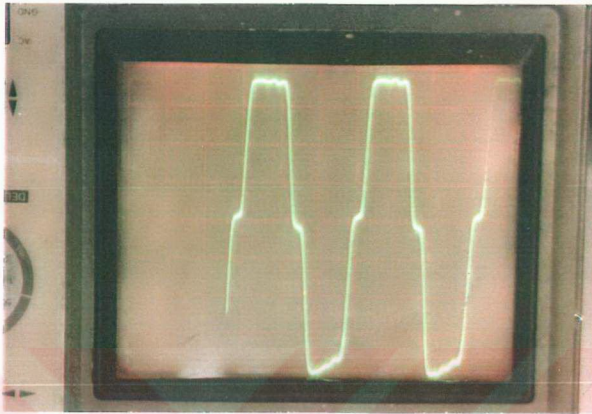


Figure 2.6. Experimentally obtained search coil voltage on an oscilloscope screen.

2.3 PERMEANCE OF THE MOTOR

The lay out flat view of the motor, permeance wave, MMF wave, flux wave, flux density wave and electromagnetic radial force waves are shown in Figure 2.7. The air gap length under the magnets differs because of existence of slots and teeth. This variation effects the permeance that is the inverse of reluctance. An enlarged section of the motor that shows slots and current carrying conductors is given in Figure 2.8.

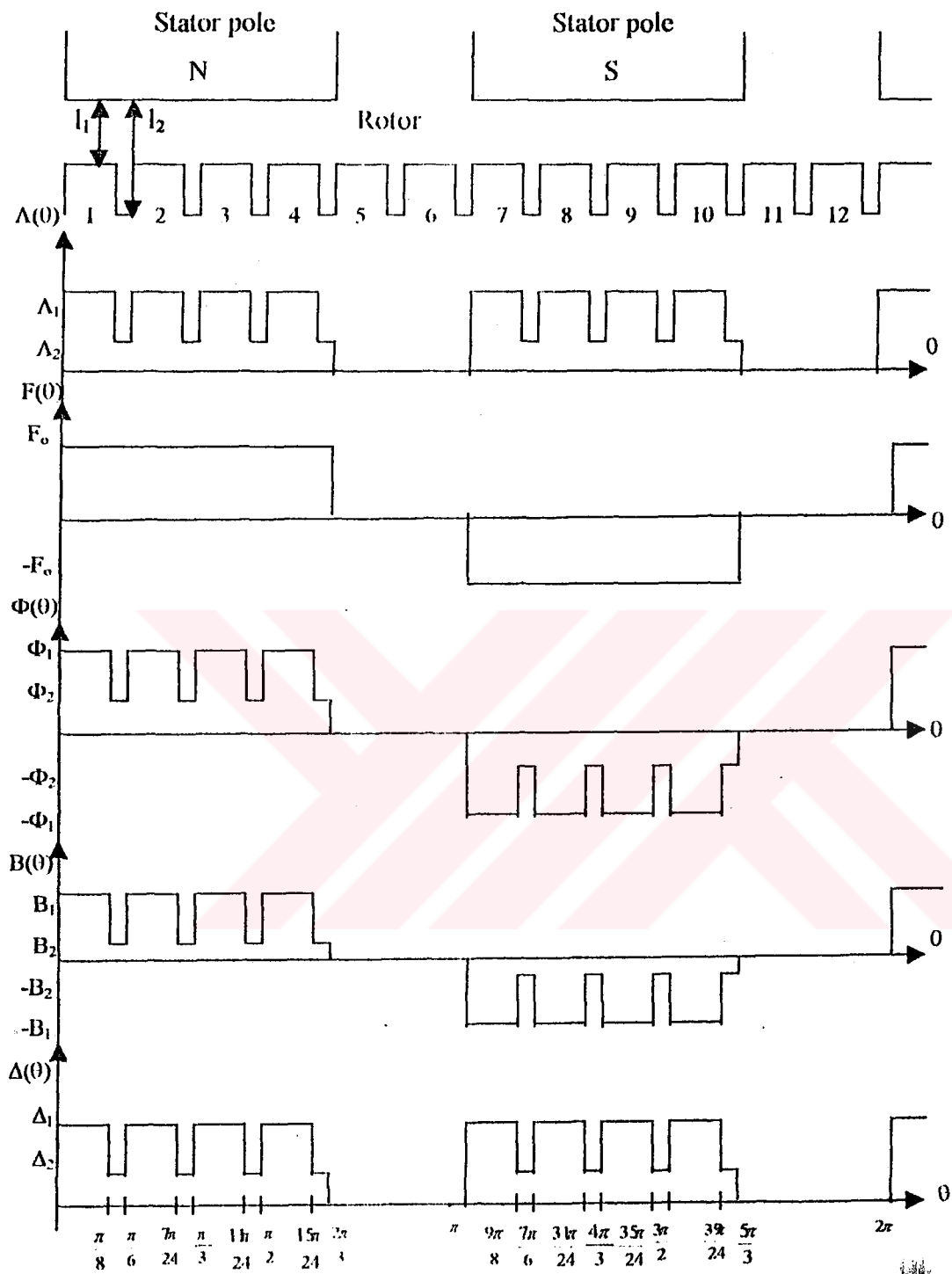


Figure 2.7. Lay out flat view of the motor, permeance waves, MMF waves, flux waves, flux density waves and electromagnetic radial forces waves.

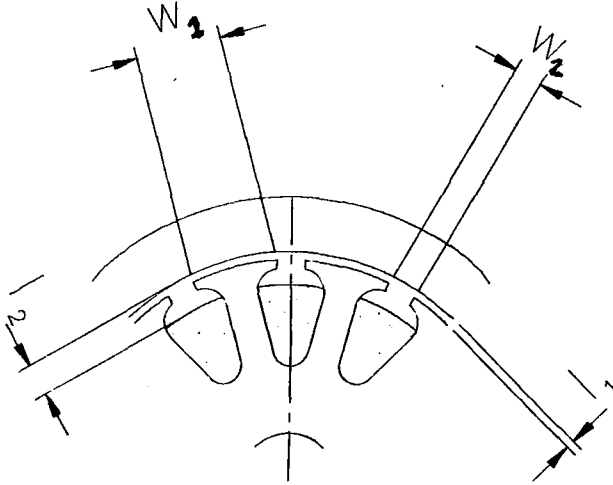


Figure 2.8 An enlarged section of the motor that shows slots and current carrying conductors

The reluctance of air gap over tooth, R_1 and reluctance of air gap over slot, R_2 are written as follows;

$$R_1 = \frac{l_1}{\mu_0 S} \quad (2.28)$$

$$R_2 = \frac{l_2}{\mu_0 S} \quad (2.29)$$

Where S is the area of the air gap and μ_0 is the magnetic permeability of space and l_1 , l_2 are air gap length over tooth and slot respectively as shown in Figure 2.8.

The permeance of air gap can be obtained by the inverse of reluctance.

$$\Lambda_1 = \frac{1}{R_1} = \frac{\mu_0 S}{l_1} \quad (2.30)$$

$$\Lambda_2 = \frac{1}{R_2} = \frac{\mu_0 S}{l_2} \quad (2.31)$$

2.4 FLUX DISTRIBUTION IN THE AIR GAP

The flux distribution that circulates thorough the armature and the air gap is obtained by the multiplication of the permeance waves and MMF produced by the magnets. It is illustrated in Figure 2.9.

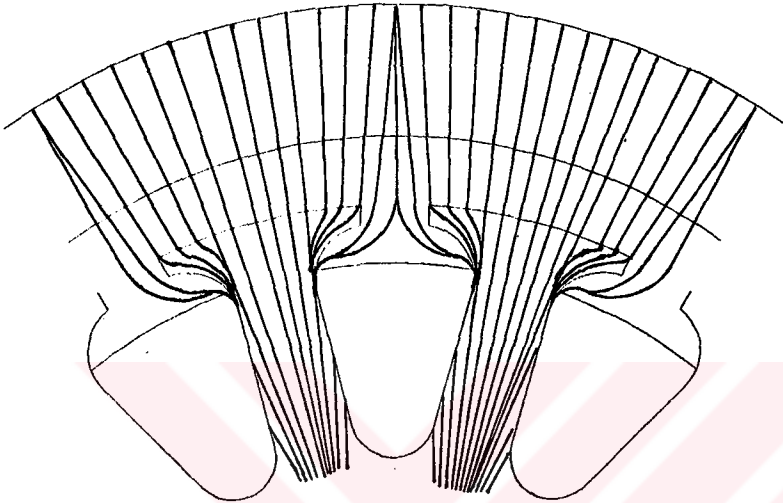


Figure 2.9. The magnetic flux path thorough the air gap and the armature laminations.

The magnetic flux in the air gap has the fluctuating wave due to the fluctuating waves of permeance between Φ_1 and Φ_2 that can be expressed as follows.

$$\Phi_1 = F_0 \Lambda_1 \quad (2.32)$$

$$\Phi_2 = F_0 \Lambda_2 \quad (2.33)$$

Where F_0 is the MMF produced by the magnets.

2.5 FLUX DENSITY DISTRIBUTION IN THE AIR GAP

The magnetic flux density in the air gap has also a fluctuating wave and it is written as follows;

$$B_1 = \frac{\Phi_1}{S} = \frac{F_0 \Lambda_1}{S} = \frac{F_0 \mu_0}{l_1} \quad (2.34)$$

$$B_2 = \frac{\Phi_2}{S} = \frac{F_0 \Lambda_2}{S} = \frac{F_0 \mu_0}{l_2} \quad (2.35)$$

The frequency spectrum of the flux density can be obtained from Fourier Transform. The general form of Fourier Series applied on the magnetic flux density distribution given in Figure 2.7 can be written as follows;

$$B(\omega t) = \frac{a_0}{2} + \sum_{n=1}^{\infty} [a_n \cos n\omega t + b_n \sin n\omega t] \quad (2.36)$$

Where;

$$\omega = 2\pi/T;$$

$$a_n = \frac{2}{T} \int_0^T B(\omega t) \cos(n\omega t) d(\omega t) ; n=0, 1, 2, \dots \quad (2.37)$$

$$b_n = \frac{2}{T} \int_0^T B(\omega t) \sin(n\omega t) d(\omega t) ; n=1, 2, 3, \dots \quad (2.38)$$

The flux density distribution in motor is symmetrical with respect to the (ωt) axis in one period. So a_0 is equal to zero. Additionally, the period, T of the flux distribution is 2π . The other coefficients can be written as follows;

$$\begin{aligned}
a_n &= \frac{2}{2\pi} \int_0^{2\pi} B(wt) \cos(nwt) d(wt) = \frac{1}{\pi} \left(\int_0^{\frac{\pi}{8}} B_1 \cos(nwt) d(wt) + \int_{\frac{\pi}{8}}^{\frac{\pi}{6}} B_2 \cos(nwt) d(wt) \right. \\
&+ \int_{\frac{\pi}{6}}^{\frac{7\pi}{24}} B_1 \cos(nwt) d(wt) + \int_{\frac{7\pi}{24}}^{\frac{\pi}{3}} B_2 \cos(nwt) d(wt) + \int_{\frac{\pi}{3}}^{\frac{11\pi}{24}} B_1 \cos(nwt) d(wt) \\
&+ \int_{\frac{11\pi}{24}}^{\frac{\pi}{2}} B_2 \cos(nwt) d(wt) + \int_{\frac{\pi}{2}}^{\frac{15\pi}{24}} B_1 \cos(nwt) d(wt) + \int_{\frac{15\pi}{24}}^{\frac{2\pi}{3}} B_2 \cos(nwt) d(wt) \\
&- \int_{\pi}^{\pi+\frac{\pi}{8}} B_1 \cos(nwt) d(wt) - \int_{\pi+\frac{\pi}{8}}^{\pi+\frac{\pi}{6}} B_2 \cos(nwt) d(wt) - \int_{\pi+\frac{\pi}{6}}^{\pi+\frac{7\pi}{24}} B_1 \cos(nwt) d(wt) \\
&- \int_{\pi+\frac{7\pi}{24}}^{\pi+\frac{\pi}{3}} B_2 \cos(nwt) d(wt) - \int_{\pi+\frac{\pi}{3}}^{\pi+\frac{11\pi}{24}} B_1 \cos(nwt) d(wt) - \int_{\pi+\frac{11\pi}{24}}^{\pi+\frac{\pi}{2}} B_2 \cos(nwt) d(wt) \\
&- \left. \int_{\pi+\frac{\pi}{2}}^{\pi+\frac{15\pi}{24}} B_1 \cos(nwt) d(wt) - \int_{\pi+\frac{15\pi}{24}}^{\pi+\frac{2\pi}{3}} B_2 \cos(nwt) d(wt) \right) \quad (2.39)
\end{aligned}$$

And;

$$\begin{aligned}
b_n &= \frac{2}{2\pi} \int_0^{2\pi} B(wt) \sin(nwt) d(wt) = \frac{1}{\pi} \left(\int_0^{\frac{\pi}{8}} B_1 \sin(nwt) d(wt) + \int_{\frac{\pi}{8}}^{\frac{\pi}{6}} B_2 \sin(nwt) d(wt) \right. \\
&+ \int_{\frac{\pi}{6}}^{\frac{7\pi}{24}} B_1 \sin(nwt) d(wt) + \int_{\frac{7\pi}{24}}^{\frac{\pi}{3}} B_2 \sin(nwt) d(wt) + \int_{\frac{\pi}{3}}^{\frac{11\pi}{24}} B_1 \sin(nwt) d(wt) \\
&+ \int_{\frac{11\pi}{24}}^{\frac{\pi}{2}} B_2 \sin(nwt) d(wt) + \int_{\frac{\pi}{2}}^{\frac{15\pi}{24}} B_1 \sin(nwt) d(wt) + \int_{\frac{15\pi}{24}}^{\frac{2\pi}{3}} B_2 \sin(nwt) d(wt) \\
&- \int_{\pi}^{\pi+\frac{\pi}{8}} B_1 \sin(nwt) d(wt) - \int_{\pi+\frac{\pi}{8}}^{\pi+\frac{\pi}{6}} B_2 \sin(nwt) d(wt) - \int_{\pi+\frac{\pi}{6}}^{\pi+\frac{7\pi}{24}} B_1 \sin(nwt) d(wt) \\
&- \int_{\pi+\frac{7\pi}{24}}^{\pi+\frac{\pi}{3}} B_2 \sin(nwt) d(wt) - \int_{\pi+\frac{\pi}{3}}^{\pi+\frac{11\pi}{24}} B_1 \sin(nwt) d(wt) - \int_{\pi+\frac{11\pi}{24}}^{\pi+\frac{\pi}{2}} B_2 \sin(nwt) d(wt) \\
&- \left. \int_{\pi+\frac{\pi}{2}}^{\pi+\frac{15\pi}{24}} B_1 \sin(nwt) d(wt) - \int_{\pi+\frac{15\pi}{24}}^{\pi+\frac{2\pi}{3}} B_2 \sin(nwt) d(wt) \right)
\end{aligned}$$

$$\begin{aligned}
& - \int_{\pi + \frac{7\pi}{24}}^{\pi + \frac{\pi}{3}} B_2 \sin(nwt) d(wt) - \int_{\pi + \frac{\pi}{3}}^{\pi + \frac{11\pi}{24}} B_1 \sin(nwt) d(wt) - \int_{\pi + \frac{11\pi}{24}}^{\pi + \frac{\pi}{2}} B_2 \sin(nwt) d(wt) \\
& - \int_{\pi + \frac{\pi}{2}}^{\pi + \frac{15\pi}{24}} B_1 \sin(nwt) d(wt) - \int_{\pi + \frac{15\pi}{24}}^{\pi + \frac{2\pi}{3}} B_2 \sin(nwt) d(wt) \quad (2.40)
\end{aligned}$$

After computing a_n and b_n from equation (2.39) and (2.40), the flux density in (2.39) can be rearranged in explicit form as follows;

$$\begin{aligned}
B(wt) = \sum_{n=1}^{\infty} \frac{1 - (-1)^n}{n\pi} & \left((B_1 - B_2) \sin n \frac{\pi}{8} + (B_2 - B_1) \sin n \frac{\pi}{6} + (B_1 - B_2) \sin n \frac{7\pi}{24} \right. \\
& + (B_2 - B_1) \sin n \frac{\pi}{3} + (B_1 - B_2) \sin n \frac{11\pi}{24} + (B_2 - B_1) \sin n \frac{\pi}{2} + (B_1 - B_2) \sin n \frac{15\pi}{24} \\
& + B_2 \sin n \frac{2\pi}{3} \left. \right) \cos nwt + \left(B_1 + (B_2 - B_1) \cos n \frac{\pi}{8} + (B_1 - B_2) \cos n \frac{\pi}{6} \right. \\
& + (B_2 - B_1) \cos n \frac{7\pi}{24} + (B_1 - B_2) \cos n \frac{\pi}{3} + (B_2 - B_1) \cos n \frac{11\pi}{24} + (B_1 - B_2) \cos n \frac{\pi}{2} \\
& + (B_2 - B_1) \cos n \frac{15\pi}{24} - B_2 \cos n \frac{2\pi}{3} \left. \right) \sin nwt \quad (2.41)
\end{aligned}$$

2.6 ELECTROMAGNETIC RADIAL FORCES

(BINNS, K., J., & LAWRENSON, P., J., & TROWBRIDGE, C., W., 1995, *The Analytical and Numerical Solution of Electric and Magnetic Fields*, 1st edition, John Wiley & Sons) Consider a region 1 of permeability $\mu_1\mu_0$ separated from a region 2 of permeability $\mu_2\mu_0$ by a boundary of arbitrary shape given in Figure 2.10. At any point on the boundary, let H_n be the normal component of the applied field strength, i.e. the field strength due to all the field sources which may be in either or both of the regions in the absence of polarised media. The effect of the polarised media can be accounted for by a normal component field H'_n at the boundary, and considered to act in the same direction as H_n in region 1.

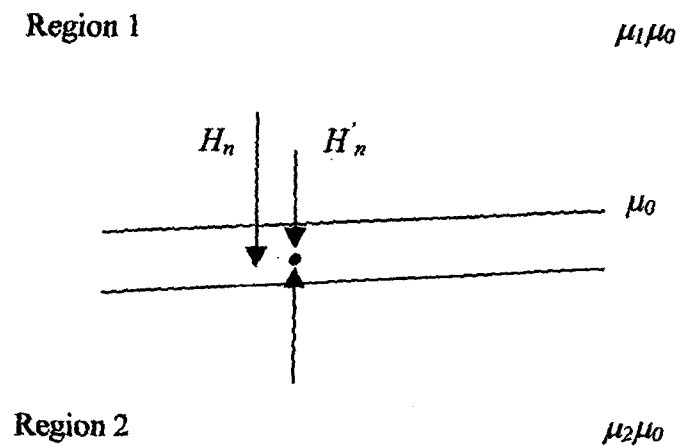


Figure 2.10. Two different regions separated by a boundary.

Thus the resultant normal field at a point on boundary $H_n + H'_n$ in region and $H_n - H'_n$ in region 2, and since the normal component of flux is continuous across the boundary it is necessary that

$$\mu_1(H_n + H'_n) = \mu_2(H_n - H'_n) \quad (2.42)$$

or

$$H'_n = \frac{\mu_2 - \mu_1}{\mu_2 + \mu_1} H_n \quad (2.43)$$

The surface pole density δ_s which gives rise, in a region of permeability μ_0 , to the components H'_n and so to the effect of the boundary, is found simply. Since flux passes equally in each of the two directions normal to the boundary,

$$\delta_s = 2\mu_0 H'_n \quad (2.44)$$

and so, eliminating H'_n between equations (2.42) and (2.43), δ_s is related to the applied field by;

$$\delta_s = 2\mu_0 \left(\frac{\mu_2 - \mu_1}{\mu_2 + \mu_1} \right) H_n \quad (2.45)$$

For the calculation of force, it is convenient to express the pole density in terms of resultant field strength in region 1, H_{n1} . This equals $H_n + H'_n$ and from equations (2.43) and (2.45) it is seen that,

$$\delta_s = \frac{\mu_0}{\mu_2} (\mu_2 - \mu_1) H_{n1} \quad (2.46)$$

A method, for the calculating total force on a boundary, is based on a consideration of the force exerted on the surface pole distribution which accounts for the influence of the boundary on the external field. The method does not give the force distribution for a piece of iron but, since the external field is truly represented, it does give the correct value for the total force. The required surface pole distribution is given by equation (2.46) in terms of H_{n1} .

Now the normal component of force per unit length Δ_n acting on the surface poles is given by

$$\Delta_n = H_n \delta_s \quad (2.47)$$

Where H_n is the applied normal field strength. The tangential component of force per unit length Δ_T is given by

$$\Delta_T = H_{T1} \delta_s \quad (2.48)$$

Where H_{T1} is the tangential field strength. From equation (2.43);

$$H_n = H_{n1} \left(\frac{\mu_2 - \mu_1}{2\mu_2} \right) \quad (2.49)$$

Hence substituting for δ_s from equation (2.46) in equation (2.47) gives

$$\Delta_n = \frac{1}{2} \mu_0 \left(1 - \frac{\mu_1^2}{\mu_2^2} \right) H_n^2 \quad (2.50)$$

And equation in (2.48) gives

$$\Delta_n = \frac{\mu_0}{\mu_2} (1 - \mu_1) H_n H_{T1} \quad (2.51)$$

When the boundaries are so highly permeable that it can be assumed that H is zero inside the iron boundary, a simple method may be used. The magnetic forces act only on the surface poles, and since $\mu_2 = \infty$, equations (2.50) and (2.51) become

$$\Delta_n = \frac{1}{2} \mu_0 H_n^2 = \frac{B_n^2}{2\mu_0} \quad (2.52)$$

and

$$\Delta_T = 0 \quad (2.53)$$

Because of the slotting structure of the armature the electromagnetic radial forces has a fluctuating between the values given as follows;

$$\Delta_1 = \frac{B_1^2}{2\mu_0} \quad (2.54)$$

$$\Delta_2 = \frac{B_2^2}{2\mu_0} \quad (2.55)$$

The harmonics of radial forces that have effect on the noise and the vibration can be similarly obtained from Fourier Transform. The general form of Fourier Series of electromagnetic radial force shown in Figure 2.7 can be written as follows;

$$\Delta(\omega t) = \frac{a_0}{2} + \sum_{n=1}^{\infty} [a_n \cos n\omega t + b_n \sin n\omega t] \quad (2.56)$$

Where;

$$a_n = \frac{2}{T} \int_0^T \Delta(\omega t) \cos(n\omega t) d(\omega t) ; n=0, 1, 2, \dots \quad (2.57)$$

$$b_n = \frac{2}{T} \int_0^T \Delta(\omega t) \sin(n\omega t) d(\omega t) ; n=1, 2, 3, \dots \quad (2.58)$$

The period, T of the electromagnetic radial force distribution is π . The coefficient can be calculated as follows;

$$\begin{aligned} a_0 &= \frac{2}{\pi} \int_0^{\pi} \Delta(\omega t) d(\omega t) = \frac{2}{\pi} \left(\int_0^{\frac{\pi}{8}} \Delta_1 d(\omega t) + \int_{\frac{\pi}{8}}^{\frac{\pi}{6}} \Delta_2 d(\omega t) + \int_{\frac{\pi}{6}}^{\frac{7\pi}{24}} \Delta_1 d(\omega t) + \int_{\frac{7\pi}{24}}^{\frac{\pi}{3}} \Delta_2 d(\omega t) \right. \\ &\quad \left. + \int_{\frac{\pi}{3}}^{\frac{11\pi}{24}} \Delta_1 d(\omega t) + \int_{\frac{11\pi}{24}}^{\frac{\pi}{2}} \Delta_2 d(\omega t) + \int_{\frac{\pi}{2}}^{\frac{15\pi}{24}} \Delta_1 d(\omega t) + \int_{\frac{15\pi}{24}}^{\frac{2\pi}{3}} \Delta_2 d(\omega t) \right) = \frac{3\Delta_1 + \Delta_2}{3} \end{aligned} \quad (2.59)$$

$$\begin{aligned} a_n &= \frac{2}{\pi} \int_0^{\pi} \Delta(\omega t) \cos(n\omega t) d(\omega t) = \frac{2}{\pi} \left(\int_0^{\frac{\pi}{8}} \Delta_1 \cos(n\omega t) d(\omega t) + \int_{\frac{\pi}{8}}^{\frac{\pi}{6}} \Delta_2 \cos(n\omega t) d(\omega t) \right. \\ &\quad \left. + \int_{\frac{\pi}{6}}^{\frac{7\pi}{24}} \Delta_1 \cos(n\omega t) d(\omega t) + \int_{\frac{7\pi}{24}}^{\frac{\pi}{3}} \Delta_2 \cos(n\omega t) d(\omega t) + \int_{\frac{\pi}{3}}^{\frac{11\pi}{24}} \Delta_1 \cos(n\omega t) d(\omega t) \right. \\ &\quad \left. + \int_{\frac{11\pi}{24}}^{\frac{\pi}{2}} \Delta_2 \cos(n\omega t) d(\omega t) + \int_{\frac{\pi}{2}}^{\frac{15\pi}{24}} \Delta_1 \cos(n\omega t) d(\omega t) + \int_{\frac{15\pi}{24}}^{\frac{2\pi}{3}} \Delta_2 \cos(n\omega t) d(\omega t) \right) \end{aligned}$$

$$+ \int_{\frac{11\pi}{24}}^{\frac{\pi}{2}} \Delta_2 \cos(nwt) d(wt) + \int_{\frac{\pi}{2}}^{\frac{15\pi}{24}} \Delta_1 \cos(nwt) d(wt) + \int_{\frac{15\pi}{24}}^{\frac{2\pi}{3}} \Delta_2 \cos(nwt) d(wt) \quad (2.60)$$

and;

$$\begin{aligned} b_n &= \frac{2}{\pi} \int_0^{2\pi} \Delta(wt) \sin(nwt) d(wt) = \frac{2}{\pi} \left(\int_0^{\frac{\pi}{8}} \Delta_1 \sin(nwt) d(wt) + \int_{\frac{\pi}{8}}^{\frac{\pi}{6}} \Delta_2 \sin(nwt) d(wt) \right. \\ &+ \int_{\frac{\pi}{6}}^{\frac{7\pi}{24}} \Delta_1 \sin(nwt) d(wt) + \int_{\frac{7\pi}{24}}^{\frac{\pi}{3}} \Delta_2 \sin(nwt) d(wt) + \int_{\frac{\pi}{3}}^{\frac{11\pi}{24}} \Delta_1 \sin(nwt) d(wt) \\ &+ \int_{\frac{11\pi}{24}}^{\frac{\pi}{2}} \Delta_2 \sin(nwt) d(wt) + \int_{\frac{\pi}{2}}^{\frac{15\pi}{24}} \Delta_1 \sin(nwt) d(wt) + \left. \int_{\frac{15\pi}{24}}^{\frac{2\pi}{3}} \Delta_2 \sin(nwt) d(wt) \right) \quad (2.61) \end{aligned}$$

Finally;

$$\begin{aligned} \Delta(t) &= \frac{3\Delta_1 + \Delta_2}{6} + \sum_{n=1}^{\infty} \frac{2}{n\pi} \left(\left((\Delta_1 - \Delta_2) \sin n \frac{\pi}{8} + (\Delta_2 - \Delta_1) \sin n \frac{\pi}{6} + (\Delta_1 - \Delta_2) \sin n \frac{7\pi}{24} \right. \right. \\ &+ (\Delta_2 - \Delta_1) \sin n \frac{\pi}{3} + (\Delta_1 - \Delta_2) \sin n \frac{11\pi}{24} + (\Delta_2 - \Delta_1) \sin n \frac{\pi}{2} + (\Delta_1 - \Delta_2) \sin n \frac{15\pi}{24} \\ &+ \left. \Delta_2 \sin n \frac{2\pi}{3} \right) \cos nwt + \left(\Delta_1 + (\Delta_2 - \Delta_1) \cos n \frac{\pi}{8} + (\Delta_1 - \Delta_2) \cos n \frac{\pi}{6} \right. \\ &+ \left. (\Delta_2 - \Delta_1) \cos n \frac{15\pi}{24} - \Delta_2 \cos n \frac{2\pi}{3} \right) \sin nwt \quad (2.62) \end{aligned}$$

The vibration and the noise radiated from an electric motor are related to the electromagnetic radial forces. The air gap flux density and electromagnetic radial forces are plotted with respect to the (wt) for the first 40 harmonics in Figure 2.11 and 2.12, respectively.

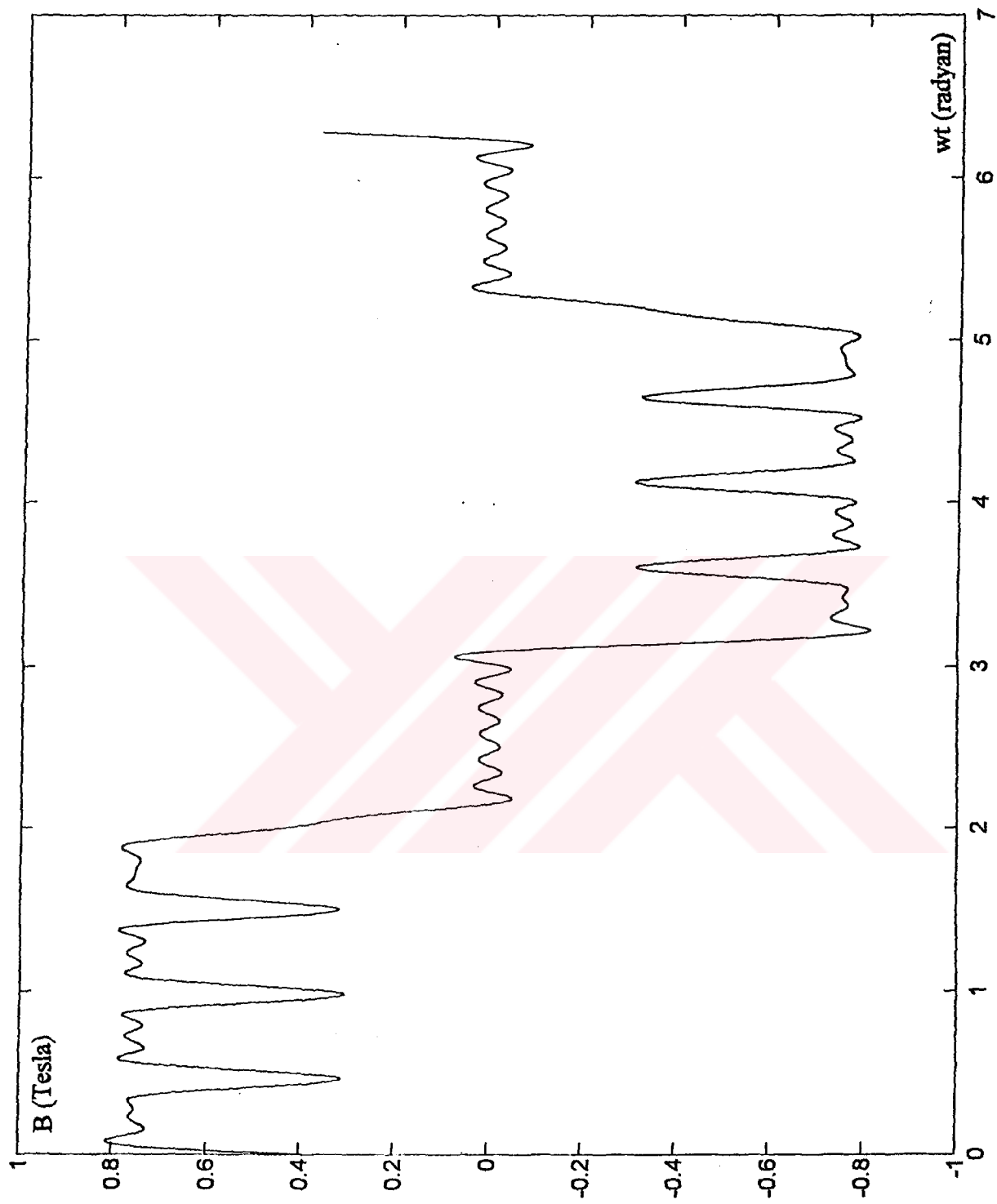


Figure 2.11 Air gap flux density

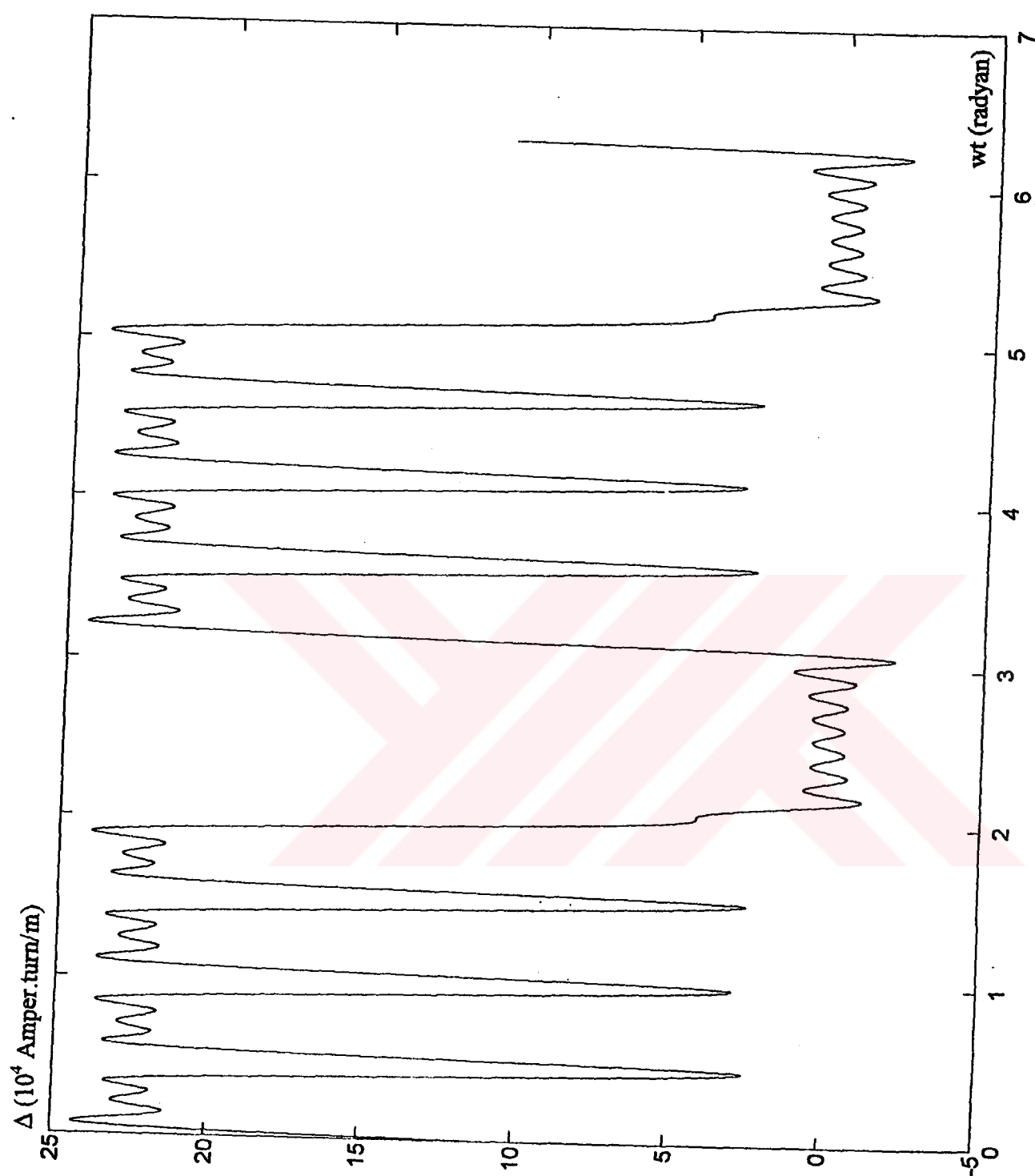


Figure 2.12 Electromagnetic radial forces

CHAPTER THREE

NOISE AND VIBRATION

In this chapter the noise and the vibration produced in wheelchair will be discussed. First, the basic phenomena of the sound waves is given. After that the noise and vibration sources in the wheelchair motor are described. Finally, the measuring devices are presented.

3.1 SOUND WAVES

(RESNICK, H., 1979, *Physics, 1st edition, John Wiley & Sons*) All sources of sound consist of some object which vibrates. These vibrations cause pressure variations in the surrounding medium (usually air) resulting in sound waves at the same frequency. In other words, the frequency of sound is determined by the source and the corresponding wavelength of the sound wave is determined by the velocity of sound in the medium and the frequency. The wavelength of the associated wave in the source is determined by the velocity of waves in the source and need not be the same as that of the sound. For this reason, in order to identify the frequency spectrum of noise, the frequency spectrum of vibration can be taken into account .

Sound waves are longitudinal mechanical waves which may be propagated in solids, liquids and gases. What one usually calls sound waves are audible sound waves and these comprise only a small fraction of the frequency range possible for longitudinal mechanical waves. This range and its upper and lower limits are shown in Figure 3.1. Also, the appropriate name of each zone are given in the same Figure.

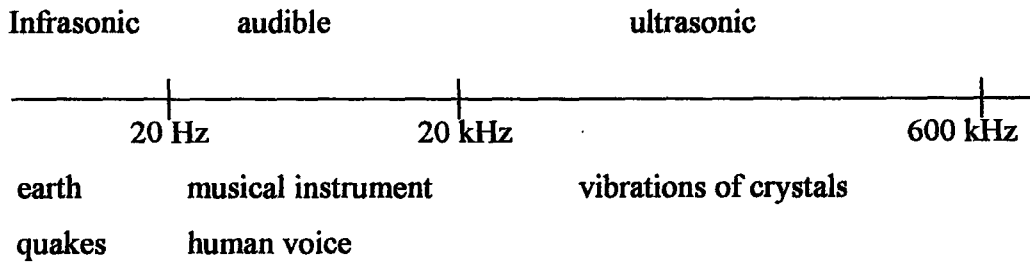


Figure 3.1 Frequency range of longitudinal mechanical waves.

As seen in Figure 3.1 the audible noise range is the small portion of whole range. Additionally, many people cannot hear up to 15 kHz. So the upper limit of the audible noise range in wheelchair can be assumed within 15 kHz. Based on this assumption we can ignore frequency components higher than 15 KHz.

3.2 THE NOISE AND THE VIBRATION SOURCE IN WHEELCHAIR MOTOR

A complete motor is shown in Figure 3.2.

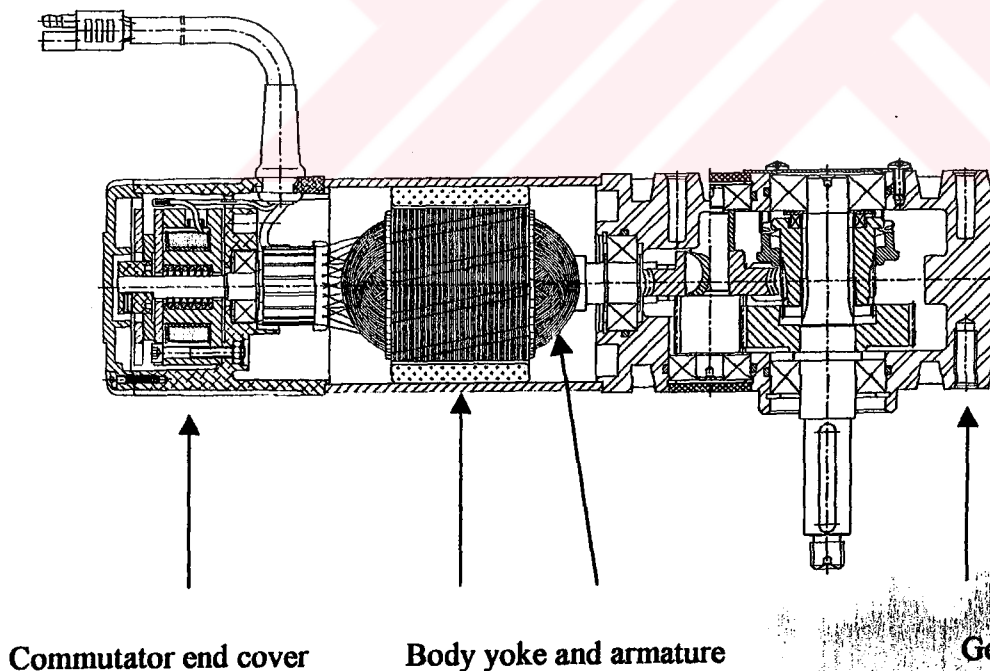


Figure 3.2 Electric motor used in the wheelchair.

The electric motor used in wheelchair consists of commutator end cover, armature, body yoke and gear. The each part of electric motor is going to be individually explained in this chapter and the effect on the noise of them will be dealt with.

3.2.1 COMMUTATOR END COVER

Commutator end cover has been moulded with plastic material that is resistant against to temperature and shock. It consists of brush holders, brushes, an electromechanical brake, suppression coils and a capacitor.

This part of motor produce main part of noise in the audible range. The main noise propagates from two brushes that consist of pressed carbon powder. There are twenty-four segments on the commutator and the brushes touch each segment in turn to maintain armature current. While the motor is rotating commutator surface rubs to the each brush and a loud noise that depends on the rotating speed, the surface finish of commutator and the carbon quality of the brushes is produced. Additionally, if the natural frequency of the plastic material or one of the components assembled into the cover coincide to one of the vibration frequencies the resonance occurs and the noise become to be more significant. In order to avoid this handicap the commutator end cover is moulded with high density materials for shifting its natural frequency and all components inside are well-connected. However, the noise radiated from the commutator end cover is determined but, the detailed analysis is excluded out of the subject of this thesis.

3.2.2 BODY YOKE AND ARMATURE

Body yoke is a round steel that two permanent magnets are stuck to its inner side. The field MMF explained in the above Chapter is produced by these two polarised magnets N and S. The yoke and two magnets stuck to its inner surface are shown in Figure 3.3.

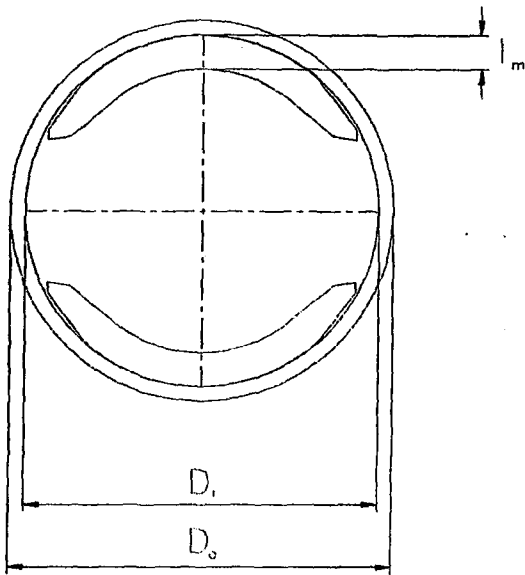


Figure 3.3 Body yoke and magnets.

The armature is the rotating part of the permanent magnet dc electric motor. It consists of a fixed length of stack as called lamination, current conductors, commutator and shaft. The view of an armature is given in Figure 3.4.

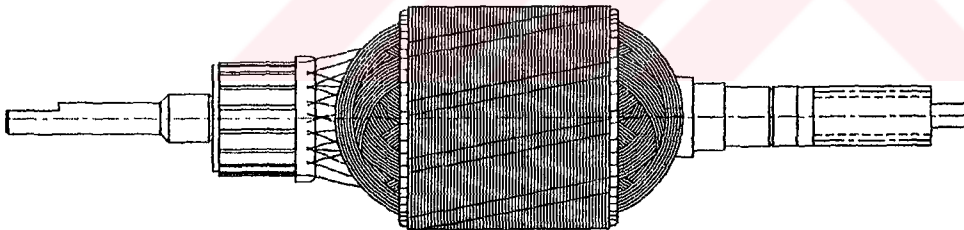


Figure 3.4 Armature of permanent magnet dc machine.

The armature is inserted into the body yoke under the magnets. In this installation some amount of air gap between the armature and the magnets occurs and the armatures can freely rotate in this air gap. In the analysis the noise sources in electric motors is derived from the air gap actions. A cross section view of the motor showing the lamination with the current carrying conductors, magnets, and yoke is shown in Figure 3.5.

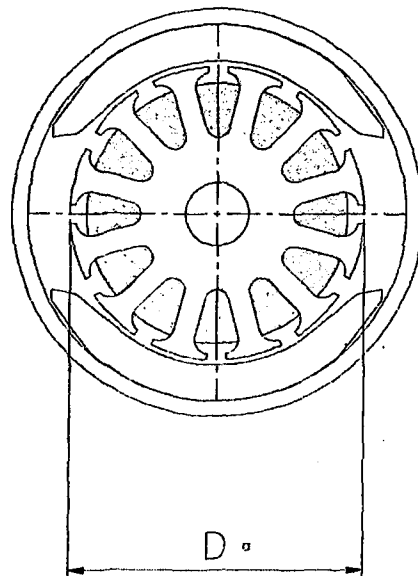


Figure 3.5. A cross section view of the motor

3.2.3 GEAR

The electric motor used in wheelchair has been coupled to a fixed gear. The gear system generally consists of one or more gears, bearings, housing and other small components. The goal of using gear system is to increase the moment and decrease the speed of the motor to the desired level. So the gear ratio of the system has been defined at the beginning. The ratio of our gear system is designed as $1/28.80$. Its meaning that the moment of the output shaft of the motor is 28.80 times smaller than the moment of the gear or the speed of the shaft of the motor is 28.80 times bigger than the speed of the gear.

The noise radiated from the gear depends on several reasons. One is the surface on each teeth of the gear. This surface has to be as smooth as possible. The other reason of the noise is the eccentricity of gear. In the case a gear eccentrically works with the other gears together in the housing and this causes the noise. An important factor of the noise derived from gear is the air gap that is called back slash between the tooth checks. The electromagnetic behaviour of motor explained above significantly effects on the gear noise. Because the moment pulsation on the motor

torque that depends on the changes into the electromagnetic flux apply a fluctuating force to the input of the gear. In the case the back slash of tooth produces more noise harmonics depending of this pulsation. However, the noise caused by the gears is also excluded out of the subject of the thesis.

3.3 MEASURING DEVICES

The frequency spectrum of the noise signal has a role on the identifying of the noise sources. The frequency of each harmonic in Fourier Transform gives us the information where the noise occurs. For this reason a Data Acquisition System has been used to acquire and to process the actual noise. The configuration of this system is given in Figure 3.6.

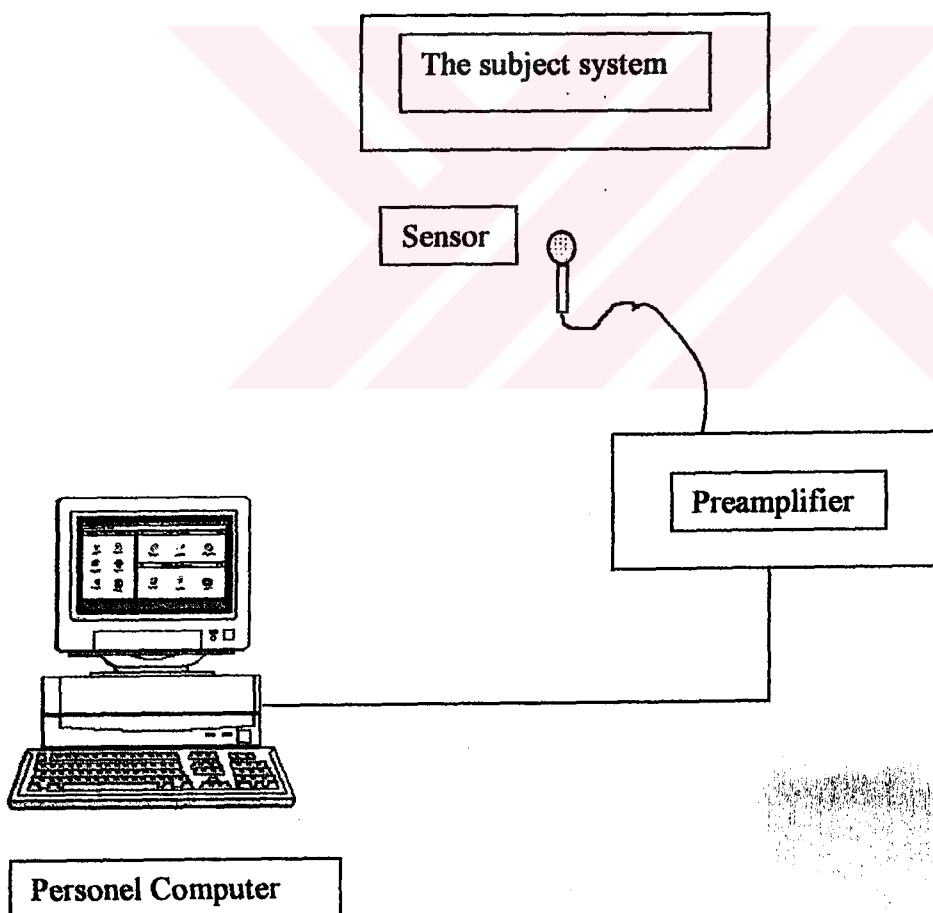


Figure 3.6. Configuration of data acquisition system

The test laboratory has been furnished from anechoic material that can absorb the reflecting noise and reduces the environmental effects. A photograph of the measuring device is shown in Figure 3.7.



Figure 3.7. Experimental set up.

3.3.1 SENSORS

Two different sensors have been used in the experiments. One is noise sensor for the acquiring the noise signals radiated from the system and the other is vibration sensor.

3.3.1.1 NOISE SENSOR

Noise sensor is a simple condenser microphone that collects the noise and converts it to electrical signal. In order to reduce the effect of the electromagnetic interference the lead between the microphone and preamplifier is used with the aluminium coated type. Additionally, the band with of microphone has been chosen as large as possible to avoid from its filtering effect. So a microphone that is capable of working between 45 Hz and 50 kHz has been chosen.

3.3.1.2 VIBRATION SENSOR

An electrodynamic vibration velocity pickup and its measuring device named VIBROMETER 20 have been used to measure the vibration signal. This is a battery operated, portable measuring instrument. It measures the vibration, which is done by its magnet mounting probe, in the frequency range of 10 Hz to 1000 Hz. It can provide the vibration signals from the BNC socket to oscilloscope. This analogue output has been directed to our Data Acquisition System as an input. The detailed information of VIBROMETER 20 is given in Appendix A.

3.3.2 PREAMPLIFIER

The level of signal coming from the sensor can be small. Therefore, a preamplifier having 16 channels devoted for different sensor types classified with strain-gage, magnetic, microphone and ceramic has been used to amplify the signal. The microphone type channel has been used in the experiments. The gain of each input channel can be individually set into the desired range. The connection to the PC is provided with the aluminium coated cable.

3.3.3 PERSONAL COMPUTER

This is an ordinary personal computer that has a Pentium 100 microprocessor, a colour monitor, and other peripheral devices has been adopted for the Data Acquisition System that involving both software and hardware requirements.

3.3.4 DATA ACQUISITION SYSTEM

Data Acquisition Systems are being readily used for different purposes such as noise and vibration analysis, digital signal processing, medicine equipment, laboratory and automation devices. It consists of a hardware and a software.

3.3.4.1 DATA ACQUISITION HARDWARE

The Data Acquisition Hardware is a board that has been designed to provide both analogue and digital signal to the Data Acquisition System and it was inserted to an extension slot of PC. It is chosen according to the system requirements among the similar boards which can be easily found in the marketing. For instance, when the speed of the system is critical the sampling rate and the speed of analogue to digital converter of the board are taken into account. However, the accuracy of the system is sometimes critical. In this case the board is chosen according to resolution bits that determine the resolution of board. In our system one of these boards named DAS 1600 has been used. This board has 16 input channel, 100 kHz sampling rate and 12 resolution bits.

3.3.4.2 DATA ACQUISITION SOFTWARE

In our system one of the software named DASYLAB that is icon based Windows compatible software has been used. The software can sample the analogue signal coming from Data Acquisition board within 10 kHz sampling rate and plot the signal in time domain. In our work the Fast Fourier Transform of the actual noise and

vibration signal is taken and then its frequency spectrum of them can be monitored simultaneously.

The detailed information of both DAS 1600 and DASYLAB are given in Appendix.



CHAPTER FOUR

RESULTS AND CONCLUSIONS

In this chapter the experimental results of the noise and the vibration produced in a wheelchair are presented. The Fast Fourier Transforms (FFT) of the actual noise and vibration have been obtained. The noise and vibration sources in a motor have been explained in Chapter III. Only the part of that created by magnetic field is subject of interest in this thesis.

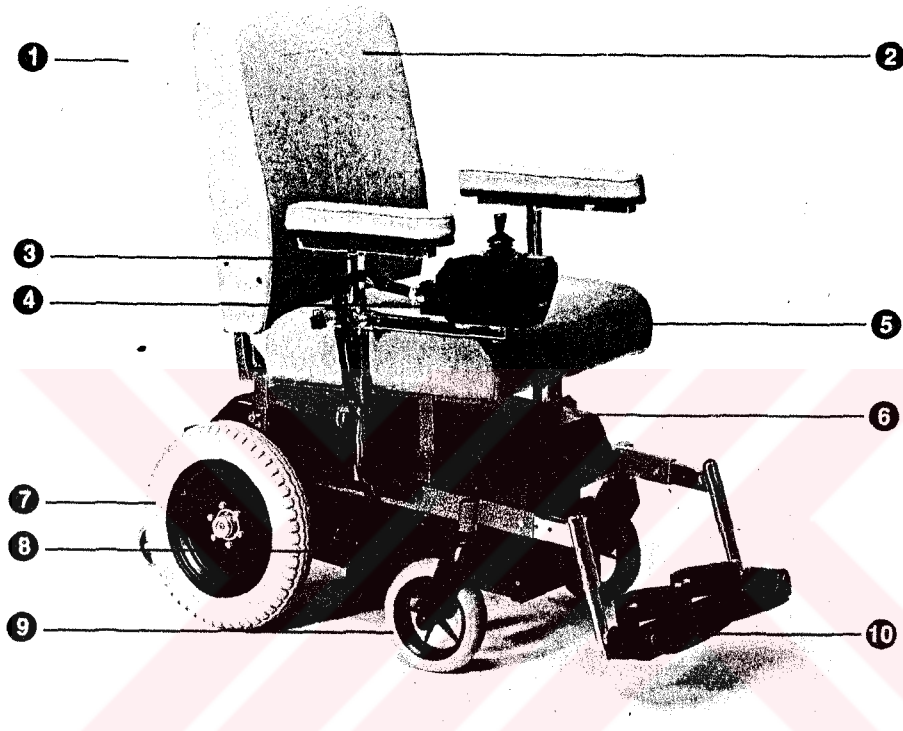
The slotting structure of the armature causes the fluctuating flux density waves in the air gap. Therefore, the electromagnetic radial forces proportional to the square of the flux density waves cause the torque pulsation that is the source of the noise and the vibration. The analytically obtained expressions for magnetic field given in Chapter II have been analysed in MATHLAB and the results are compared with the experimental ones. The routines written in MATHLAB are given in Appendix.

4.1 THE EXPERIMENTAL RESULTS

It is here noted that the motors used in the experiments are well balanced and there is no eccentricity on the armatures. Because of the periodic calibration of the vibration device it is more accurate than the noise device. Unfortunately, a general purpose microphone used for the measurement of the noise has been effected from environmental conditions. Although several types microphone have been used, a good improvement has not been obtained since the chamber is not entirely closed, yet. Therefore, the vibration spectrums are taken into account.

4.1.1 THE FFT OF THE VIBRATION OF WHEELCHAIR

A photo of an electrically powered wheelchair is given in Figure 4.1. The frequency spectrums of vibration produced in the wheelchair are given in Figure 4.2.



1. Handle for manual use
2. Adjustable backrest
3. Adjustable armrest
4. Controller
5. Adjustable seat
6. Waterproof battery enclosure
7. Rearwheel
8. Permanent magnet direct current motor
9. Castor
10. Adjustable footrest

Figure 4.1 A photo of an electrically powered wheelchair and the name of its parts.

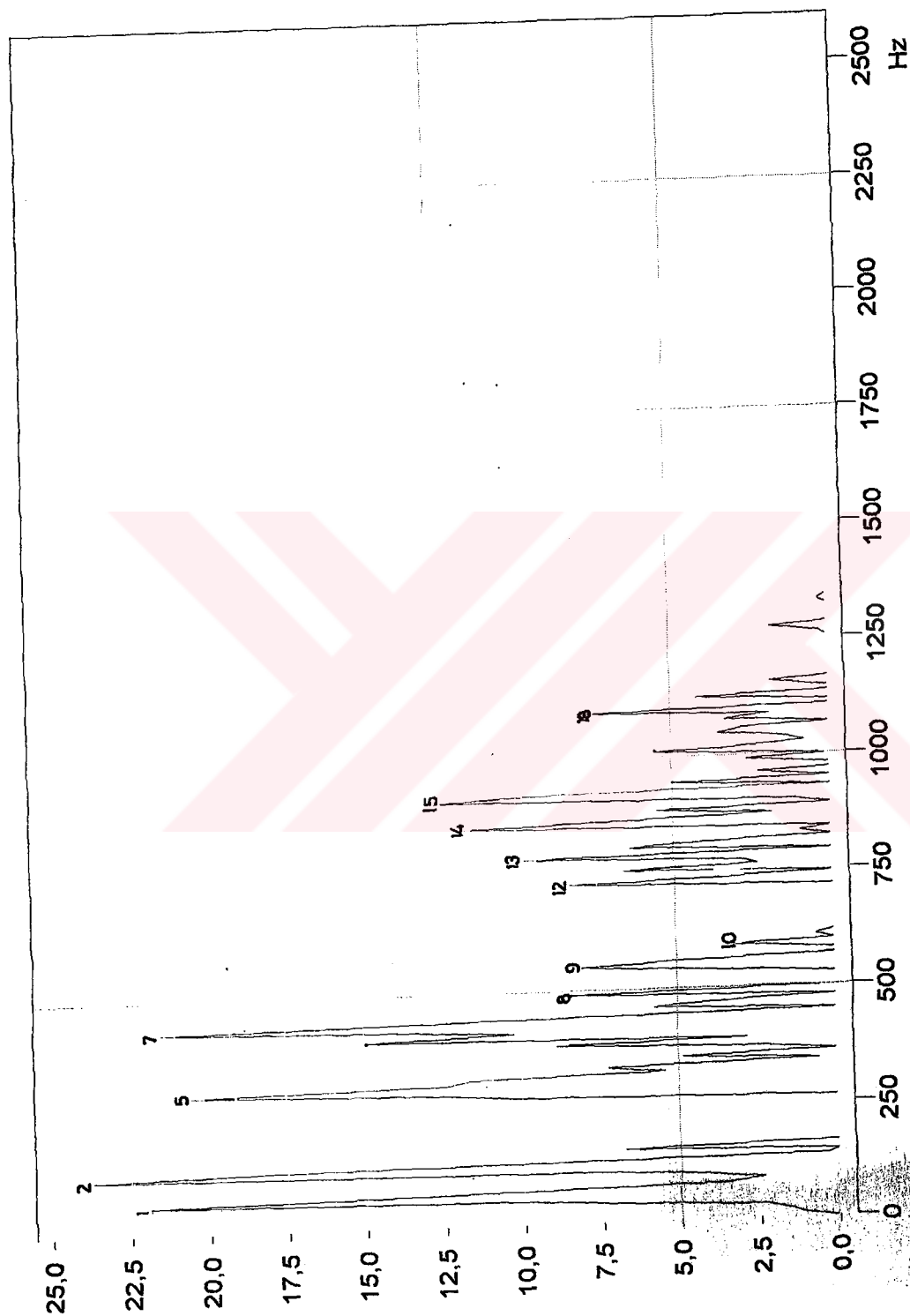


Figure 4.2. The frequency spectrum of vibration produced in wheelchair.

The frequency spectrum can be obtained while the wheelchair is operated onto a support where the wheels can rotate free. The wheels were rotated at the speed of 125 rpm. The gear ratio of the system is 1/28.8. So the motor speed is 3600 rpm. In measurement of the vibration sensor based vibration magnet is mounted onto the motor.

The effective components of frequency in the spectrum of vibration appear at 1st, 2nd, 5th, 7th, 8th, 9th, 10th, 12th, 13th, 14th, 15th, 18th times of motor speed.

4.1.2 THE FFT OF THE VIBRATION OF THE MOTOR COUPLED WITH A GEAR SYSTEM

The frequency spectrums of vibration of the motor coupled with a gear system is shown in Figure 4.3. In this test, the wheels are disconnected.

The motor is operated under the unload condition with an external voltage supply that can give adjustable purely dc voltage. The geared motor is rotated at 125 rpm so that the speed of the motor is 3600 rpm. The test voltage and current are about 19.4 Volts and 2.3 Amps, respectively. The 1st, 2nd, 4th, 8th, 10th, 12th, 13th, 16th, 19th, 20th harmonics are obtained from the spectrum analysis of vibration. The mid-components appear at the 5.6, 6.6, 8.6, 12.6, 16.6 and 17.6 harmonics. Although the effect of the gear system on the vibration is out of the subject of this thesis, it is considered that the mid-components are generated from the different number of the gear tooth.

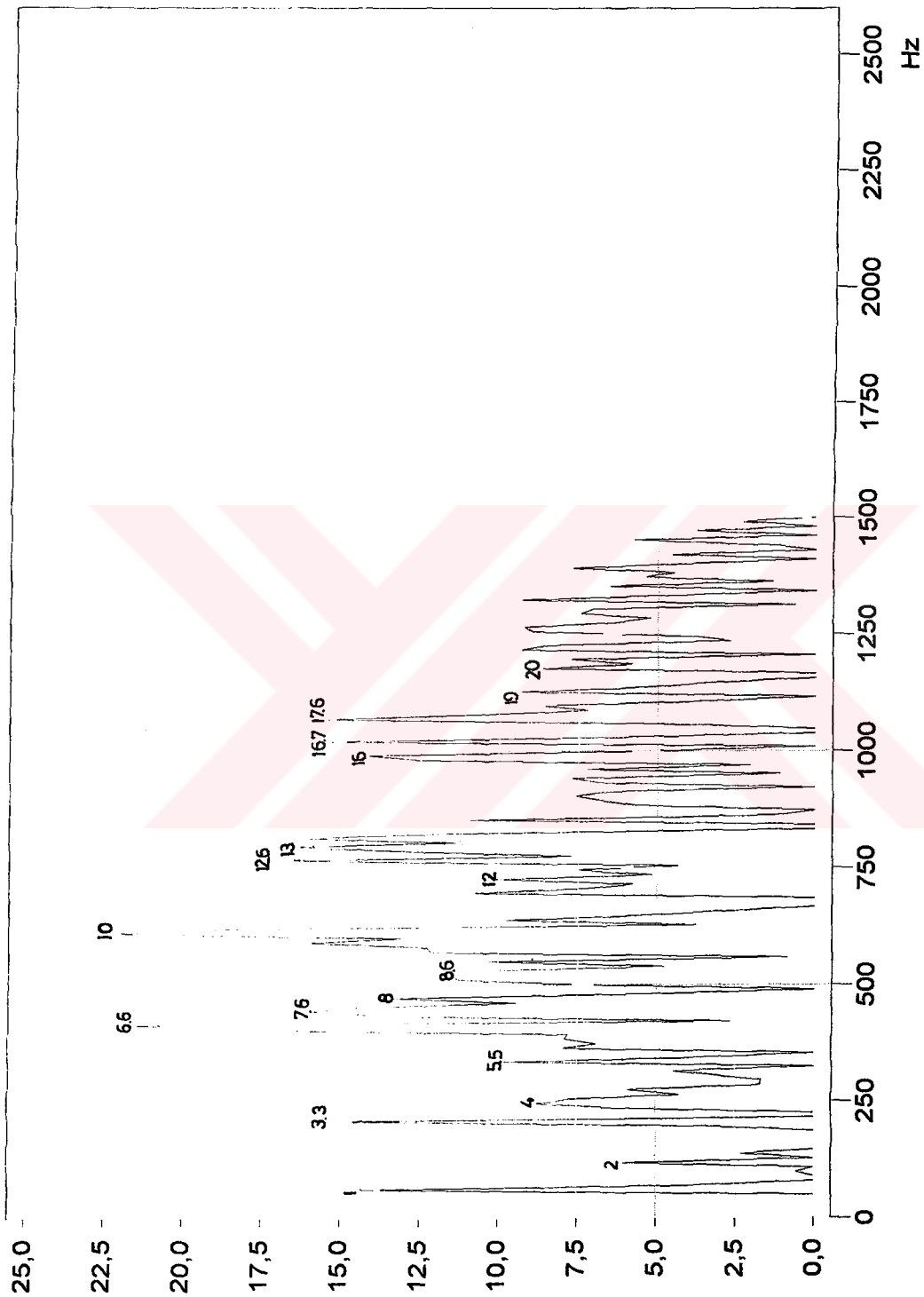


Figure 4.3. The frequency spectrum of the vibration produced in the motor coupled with the gear system.

4.1.3 THE FFT OF THE VIBRATION OF THE MOTOR WITHOUT A GEAR SYSTEM

The frequency spectrums of the vibration of the motor without a gear system is shown in Figure 4.4. The motor is rotated at 3600 rpm. The test voltage and current are about 18.6 Volts and 1.4 Amps, respectively.

The integer multiplies of fundamental on the spectrum analysis are dominant. The mid-components are disappeared and the number of the harmonics reduced.

The frequency components in the vibration spectrum at the 1st, 2nd, 4th, 6th, 8th, 10th, 11th, 12th, 14th, 17th, 24th harmonics are obtained.

4.1.4 THE FFT OF THE NOISE AND THE VIBRATION OF THE MOTOR ROTATED BY AN EXTERNAL PRIME MOVER

Since MMF produced by the armature current is small compared to MMF produced by the magnets, it is neglected for simplicity of analysis. So the rotor is rotated by an external prime mover coupled to the shaft with a flexible coupling. At the same time the brushes of the motor are taken out. First, this test was done with a rigid, screw fastened coupling but, it was seen that the coupling produces the additional noise and vibration. The flexible one is therefore, preferred.

The frequency spectrums of the noise and the vibration of the motor rotated by an external moving device are shown in Figure 4.5 and Figure 4.6, respectively. The motor is rotated at 3600 rpm. The microphone is directed to the motor and the vibration sensor inserted onto the motor.

The frequency components in the noise spectrum are at the 1st, 2nd, 3rd, 4th, 5th, 6th, 7th, 8th, 11th, 15th harmonics. The frequency components in the vibration spectrum at the 1st, 2nd, 4th, 5th, 6th, 7th, 9th, 10th, 11th, 12th harmonics are obtained.

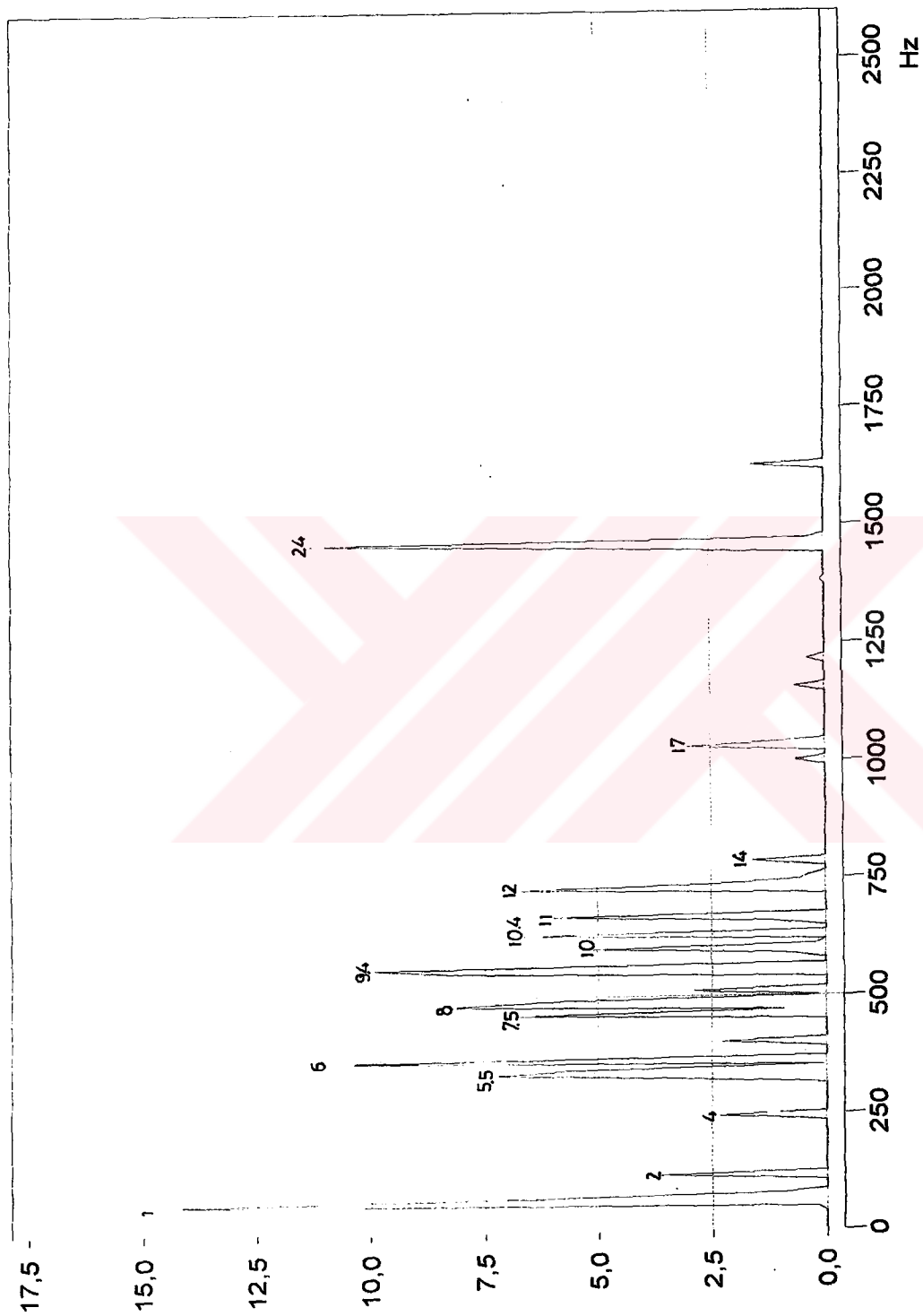


Figure 4.4. The frequency spectrum of the vibration produced in the motor without the gear system.

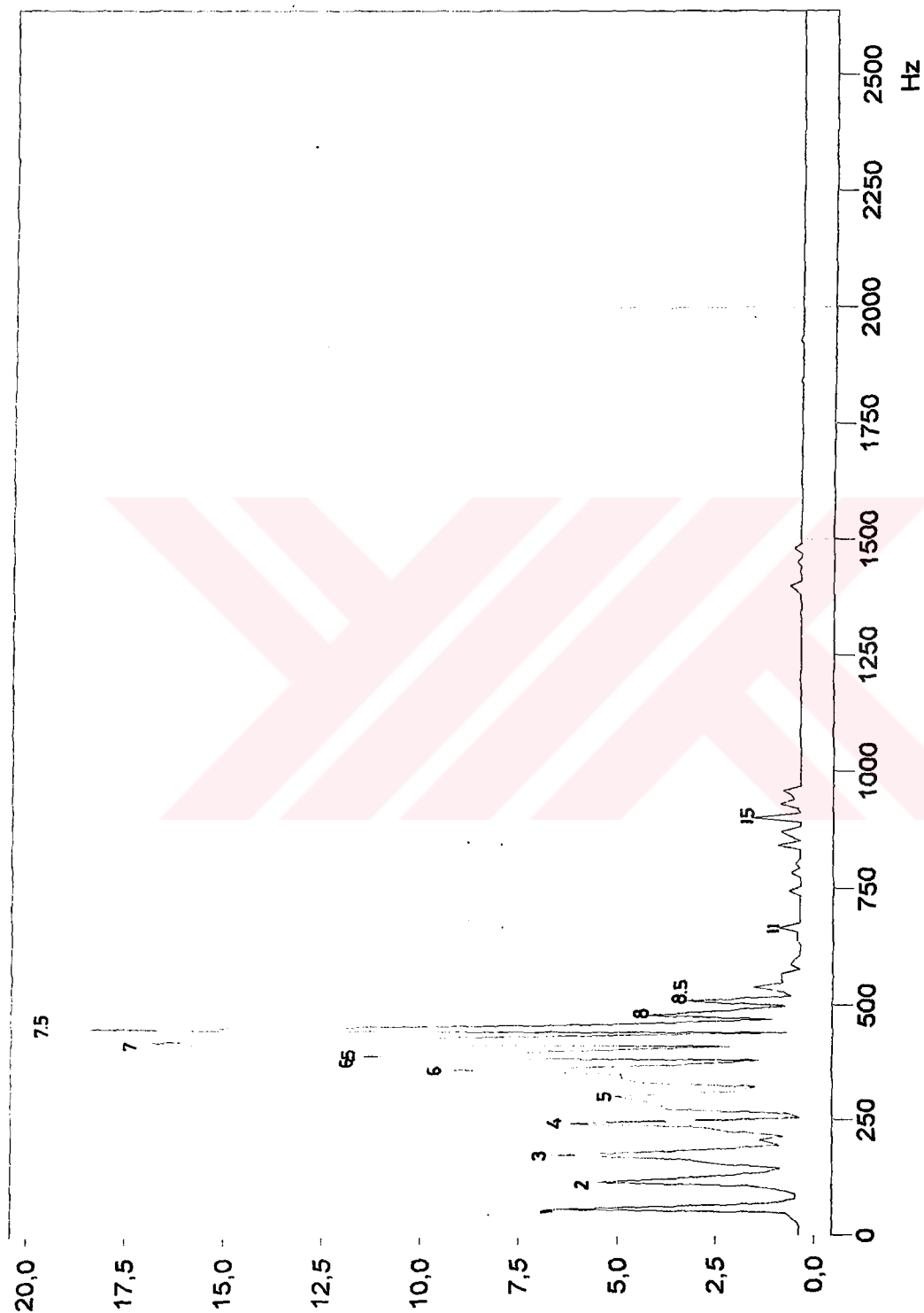


Figure 4.5. The frequency spectrum of the noise radiated from the motor rotated by an external prime mover.

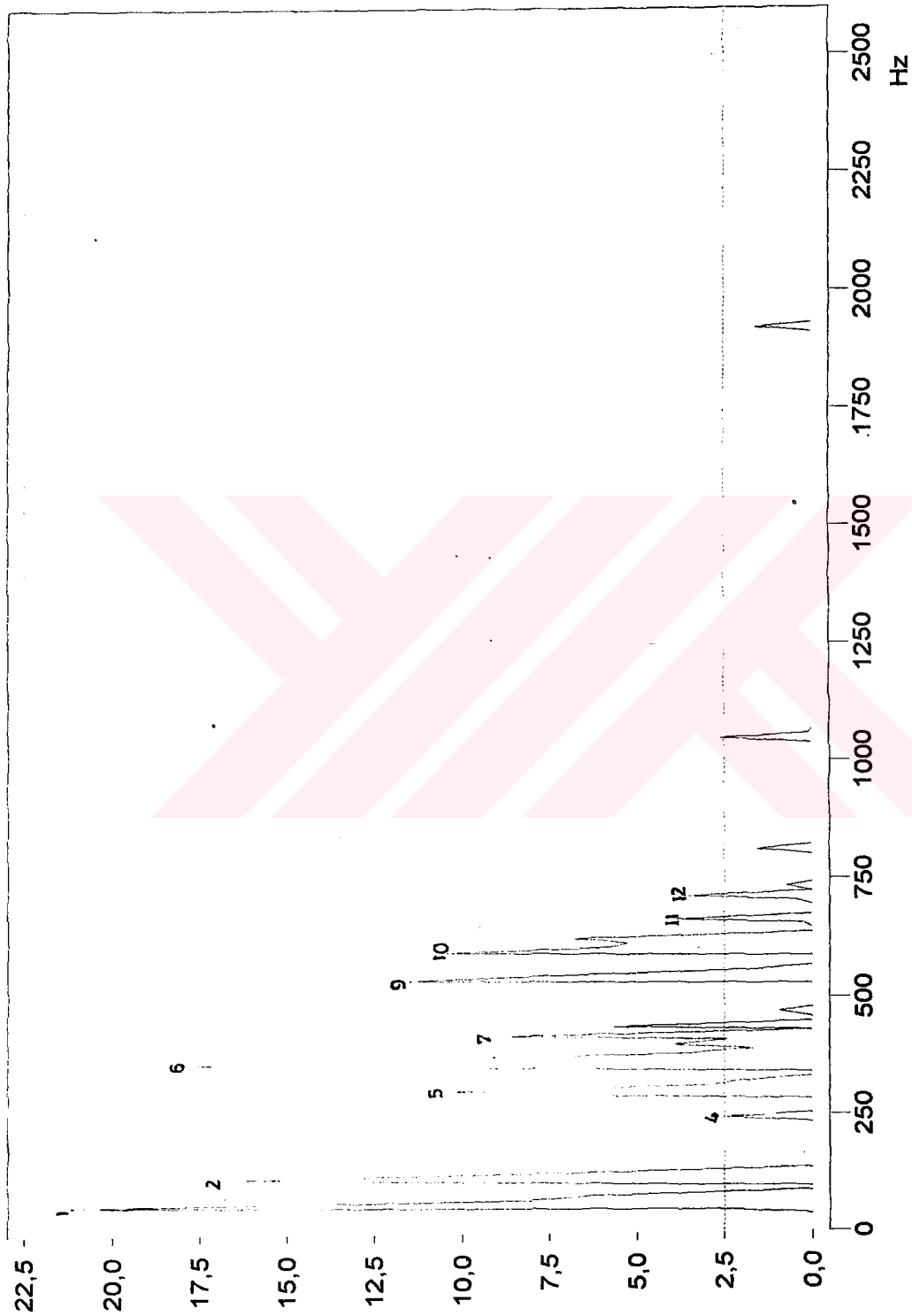


Figure 4.6. The frequency spectrum of the vibration produced in the motor rotated by an external prime mover.

4.2 THE THEORETICAL RESULTS

The electromagnetic radial forces formulated in Chapter II have been computed in MATHLAB and its FFT has been generated. The equations derived in Chapter II are calculated using the parameters measured on test motor. The value of the variables and the result of the equations are given in Table 5.

Table 5. The parameter of test motor.

Symbol	The reference equation	Value	Unit
R_1	2.28	2.612×10^5	Weber/Amper.turn
R_2	2.29	5.224×10^5	Weber/Amper.turn
A_1	2.30	0.383×10^{-5}	Amper.turn/Weber
A_2	2.31	0.192×10^{-5}	Amper.turn/Weber
F_0		599.99	Amper.turn
Φ_1	2.32	229.8×10^{-5}	Weber
Φ_2	2.33	115.2×10^{-5}	Weber
B_1	2.34	0.754	Tesla
B_2	2.35	0.377	Tesla
Δ_1	2.54	22.4×10^4	Amper.turn/m
Δ_2	2.55	5.6×10^4	Amper.turn/m

The air gap flux density and electromagnetic radial forces are plotted in time domain during a period in Figure 2.11 and Figure 2.12, respectively. The figures have been obtained by taking into account the first 40 harmonics of Fourier Transform. The FFT of the electromagnetic radial forces is given in Figure 4.7.

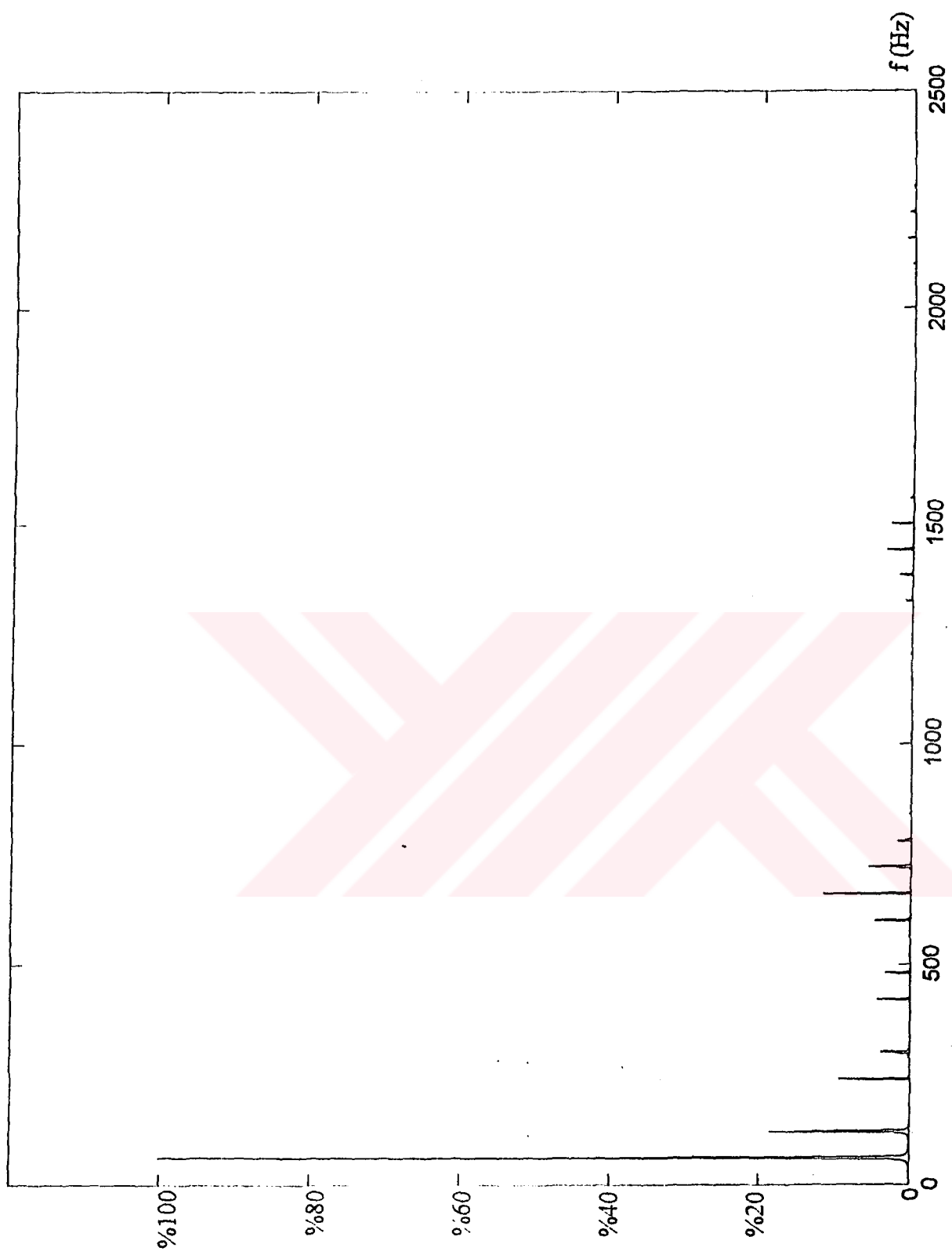


Figure 4.7 FFT of the electromagnetic radial forces.

4.3 COMPARISON BETWEEN EXPERIMENTAL AND THEORETICAL RESULTS

In Figure 4.6, the spectrum of vibration the motor driven by an external prime mover is given. FFT of the electromagnetic radial forces given in Figure 4.7 shows the similarity to Figure 4.6. In the measurements 6th, and 9th, harmonics appeared but, in the theoretically analysis of FFT, these two harmonics are disappeared.

The 3rd, 6th, 9th harmonics are equal to zero in Fourier Transform because the width of magnet called magnet angle occupies 120°. Therefore, the 3rd, 6th, 9th, 15th, 18th, 21st ... harmonics are equal to zero. If the magnet angle is 180° (if the magnets are completely stuck thorough the inner surface of the yoke) all harmonics would be appearing. At the same time the motor has a skewed armature so that the skew angle is 11°. In the analysis this has been ignored.

4.4 CONCLUSIONS

The slotting structure of the armature creates the fluctuating wave of flux density and electromagnetic radial forces. This causes vibration and noise in a permanent magnet direct current motor. In addition, the magnet angle and skew angle have effects on the harmonics of noise and vibration.

In order to analyse the harmonics of the noise and the vibration in an electric motor, the magnetic properties have to be well defined. The field MMF and the reluctance distribution have to be analysed precisely as much as it is possible. The voltage induced in search coil can be used for the verification of the magnetic analysis.

Although the measuring device needs to be improved the technique could be applied to a system wherein the noise is problem.

From this point of view the technique used in this study will be adopted to the manufacturing process for different sort of electric motors. A diagnosis of the machines having fault from the manufacturing process will be identified by using the vibration characteristic.

REFERENCES

BINNS, K., J., & LAWRENSON, P., J., & TROWBRIDGE, C., W. (1995). The Analytical and Numerical Solution of Electric and Magnetic Fields (1st edition). USA: John Wiley & Sons, Inc.

CRAIU, O., & DAN, N., & BADEA, A., E. (1995). Numerical Analysis of Permanent Magnet DC Motor Performance. IEEE Transactions on Magnetics, 31, no.6, 3500-3502.

EUROPEAN COMMITTEE FOR STANDARDISATION. (1995). Pr.EN 12184 Electrically Powered Wheelchairs, Scooters, and Their Chargers-Requirements and Test Methods. Belgium: Central Secretariat.

FITZGERALD, A., E., & KINGSLEY, C., & UMANS, S., D. (1983). Electric Machinery (4th edition). USA: McGraw-Hill.

GANGA, V., & REE, J.(1991). Electromechanical Forces and Torque in Brushless Permanent Magnet Machines. IEEE Transactions on Energy Conversion, 6 no.3, 546-552.

KOBAYASHI, T., & TAJIMA, F., & ITO, M., & SHIBUKAWA, S. (1997). Effects Of Slot Combination on Acoustic Noise from Induction Machine. IEEE Transactions on Magnetics, 33, no.2, 2101-2104.

NARAYANAN, S., S., Y., & NAIR, K., R., A., & NARAYANAN, V. (1998). Design Analysis of Permanent Magnet D.C. Motors with Differing Armature, Magnet and Yoke Lengths. IEEE Transactions on Energy Conversion, 13, no:1, 55-61.

REE, J., & BOULES, N. (1991). Magnet Shaping to Reduce Induced Voltage Harmonics in PM Machines with Surface Mounted Magnets. IEEE Transactions on Energy Conversion, 6, no:1, 155-161.

RESNICK, H. (1979). Physics (1st edition). USA: John Wiley & Sons, Inc.

ROBBINS & MYERS/ELECTRO-CRAFT (1989). DC Motors Speed Controls Servo Systems (5th edition). USA: Robbins & Myers/Electro-Craft.

TOLIYAT, H., A., & WAIKAR, S., P., & LIPO, T., A. (1998). Analysis and Simulation Of Five-Phase Synchronous Reluctance Machines Including Third Harmonic of Airgap MMF. IEEE Transactions on Industry Applications, 34, no:2, 332-339.

VERMA, S., P., & BALAN, A., (1994). Determination of Radial-Forces in Relation to Noise and Vibration Problems of Squirrel-Cage Induction Motors. IEEE Transactions on Energy Conversion, 9, no:2, 404-412.

YACAMINI, R., & CHANG, S., C. (1995). Noise and Vibration from Induction Machines Fed from Harmonic Sources. IEEE Transactions on Energy Conversion, 10, no:2, 286-292.

APPENDIX

THE FLUX DENSITY FOR 40 HARMONICS;

```
for n=1:40;
A(n)=((1-(-1)^n)/(n*pi))*(0.377)*(sin(n*pi/8)-sin(n*pi/6)
)+sin(n*7*pi/24)-sin(n*pi/3)+sin(n*11*pi/24)-sin(n*pi/2)
+sin(n*15*pi/24)+sin(n*2*pi/3));
B(n)=((1-(-1)^n)/(n*pi))*(0.377)*(-cos(n*pi/8)+2+cos(n*pi/6)
)-cos(n*7*pi/24)+cos(n*pi/3)-cos(n*11*pi/24)+cos(n*pi/2)
-cos(n*15*pi/24)-cos(n*2*pi/3));
end;
» who
```

Your variables are:

```
A          B          n
```

```
» A
```

```
A =
```

Columns 1 through 7

```
    0.3819         0    0.0000         0    -0.0555
0    0.0798
```

Columns 8 through 14

```
         0    0.0000         0    0.0048         0    -0.
0513         0
```

Columns 15 through 21

```
    0.0000         0    -0.0095         0    0.0233
0    0.0000
```

Columns 22 through 28

```
0      0.0479      0      -0.0441      0      0.
0000      0
```

Columns 29 through 35

```
-0.0153      0      0.0052      0      0.0000
0      0.0191
```

Columns 36 through 40

```
0      -0.0014      0      0.0000      0
```

» B

B =

Columns 1 through 7

```
0.6205      0      0.0000      0      0.1422
0      0.0849
```

Columns 8 through 14

```
0      0.0000      0      0.1518      0      0.
0143      0
```

Columns 15 through 21

```
0.0000      0      0.0253      0      0.0165
0      0.0000
```

Columns 22 through 28

```
0      0.0537      0      0.0494      0      0.
0000      0
```

Columns 29 through 35

```
0.0108      0      0.0139      0      0.0000
0      0.0053
```

Columns 36 through 40

```
0      0.0451      0      0.0000      0
```

» t=0:0.001:2*pi;

» B=((0.3819*cos(t))- (0.0555*cos(5*t))+(0.0798*cos(7*t)))

```
+(0.0048*cos(11*t))-(0.0513*cos(13*t))-(0.0095*cos(17*t))
)+(0.0233*cos(19*t))+(0.0479*cos(23*t))-(0.0441*cos(25*t))
)-(0.0153*cos(29*t))+(0.0052*cos(31*t))+(0.0191*cos(35*
t))-(0.0014*cos(37*t))+(0.6205*sin(t))+(0.1422*sin(5*t))
+(0.0849*sin(7*t))+(0.1518*sin(11*t))+(0.0143*sin(13*t))
+(0.0253*sin(17*t))+(0.0165*sin(19*t))+(0.0537*sin(23*t)
)+(0.0494*sin(25*t))+(0.0108*sin(29*t))+(0.0139*sin(31*t)
)+(0.0053*sin(35*t))+(0.0451*sin(37*t)));
» plot(t,B);
```



THE ELECTROMAGNETIC RADIAL FORCES FOR 40 HARMONICS

```
for n=1:40;
A(n)=(2/(n*pi))*((16.8*sin(n*pi/8))-(16.8*sin(n*pi/6))+
16.8*sin(n*7*pi/24))-(16.8*sin(n*pi/3))+16.8*sin(n*11*
pi/24))-(16.8*sin(n*pi/2))+16.8*sin(n*15*pi/24))+5.6*si
n(n*2*pi/3));
B(n)=(2/(n*pi))*(22.4-(16.8*cos(n*pi/8))+(16.8*cos(n*pi/
6))-(16.8*cos(n*7*pi/24))+(16.8*cos(n*pi/3))-(16.8*cos(n
*11*pi/24))+16.8*cos(n*pi/2))-(16.8*cos(n*15*pi/24))-(5
.6*cos(n*2*pi/3)));
end;
» who
```

Your variables are:

A B n

» A

A =

Columns 1 through 7

10.8451	-4.2566	0.0000	3.4457	-1.2397	0.	
0000	2.6753					

Columns 8 through 14

-0.3859	0.0000	3.4711	0.7748	-3.5651	-2.	
7625	-0.6081					

Columns 15 through 21

0.0000	0.1930	-0.0593	0.0000	0.7125	0.	
3804	0.0000					

Columns 22 through 28

1.5778	2.4035	0.0000	-2.2112	-1.3350	0.	
0000	-0.2717					

Columns 29 through 35

-0.4668	0.0000	0.0325	-0.0965	0.0000	0.	
2504	1.0261					

Columns 36 through 40

1.1884 -0.2303 -0.9134 0.0000 0.0772

» B

B =

Columns 1 through 7

16.9577 9.2233 0.0000 4.0107 4.1974 0.
0000 2.2568

Columns 8 through 14

3.3423 0.0000 1.8447 5.7923 3.5651 -0.
1854 -0.5537

Columns 15 through 21

0.0000 0.3342 0.4976 0.0000 0.1721 0.
8021 0.0000

Columns 22 through 28

-0.3523 1.9282 3.5651 1.7739 -0.2981 0.
0000 0.5730

Columns 29 through 35

0.1127 0.0000 0.2729 0.1671 0.0000 -0.
2280 -0.0689

Columns 36 through 40

1.1884 1.7220 0.4854 0.0000 0.6685

» t=0:0.001:2*pi;

» F1=(10.8451*cos(t))-(4.2566*cos(2*t))+(3.4457*cos(4*t))
-(1.2397*cos(5*t))+(2.6753*cos(7*t))-(0.3856*cos(8*t))+
(3.4711*cos(10*t))+(0.7748*cos(11*t))-(3.5651*cos(12*t))
-(2.7625*cos(13*t))-(0.6081*cos(14*t))+(0.193*cos(16*t))
-(0.0593*cos(17*t))+(0.7125*cos(19*t))+(0.3804*cos(20*t))
+(1.5778*cos(22*t))+(2.4035*cos(23*t))-(2.2112*cos(25*t))
-(1.335*cos(26*t))-(0.2717*cos(28*t))-(0.4668*cos(29*t))
+(0.0325*cos(31*t))-(0.0965*cos(32*t))+(0.2504*cos(34*t))
+(1.0261*cos(35*t))+(1.1884*cos(36*t))-(0.2303*cos(37*t))
-(0.9134*cos(38*t))+(0.0772*cos(40*t));

» F2=(16.9577*sin(t))+(9.2233*sin(2*t))+(4.0107*sin(4*t))
+(4.1974*sin(5*t))+(2.2568*sin(7*t))+(3.3423*sin(8*t))
+(1.8447*sin(10*t))+(5.7923*sin(11*t))+(3.5651*sin(12*t))
-(0.1854*sin(13*t))-(0.5537*sin(14*t))+(0.3342*sin(16*t))


```

)+(0.4976*sin(17*t))+(0.1721*sin(19*t))+(0.8021*sin(20*t
))- (0.3523*sin(22*t))+(1.9282*sin(23*t))+(3.5651*sin(24*
t))+(1.7739*sin(25*t))-(0.2981*sin(26*t))+(0.573*sin(28*
t))+(0.1127*sin(29*t))+(0.2729*sin(31*t))+(0.1671*sin(32
*t))-(0.228*sin(34*t))-(0.0689*sin(35*t))+(1.1884*sin(36
*t))+(1.722*sin(37*t))+(0.4854*sin(38*t))+(0.6685*sin(40
*t));
» F=(24.27)/2+F1+F2;
» plot(t,F);

```

FFT OF ELECTROMAGNETIC RADIAL FORCES

```

Z=fft(F,5120);
Pzz=Z.*conj(Z)/5120;
g=10000*(1:1250)/5120;
plot(g,Pzz(2:1251));

```



Chapter 1

INTRODUCTION

1.1 GENERAL DESCRIPTION

The DAS-1601 and DAS-1602 boards (hereinafter referred to as the DAS-1600) are multifunction, high-speed, analog and digital interface boards for the IBM PC/XT/AT, and compatible computers. The DAS-1600 installs directly into a computer expansion slot, turning the computer into a fast, precise, data acquisition and signal analysis instrument. These boards use multilayer construction with integral ground plane to minimize noise and crosstalk at high frequencies. Figure 1-1 shows a block diagram of the DAS-1600.

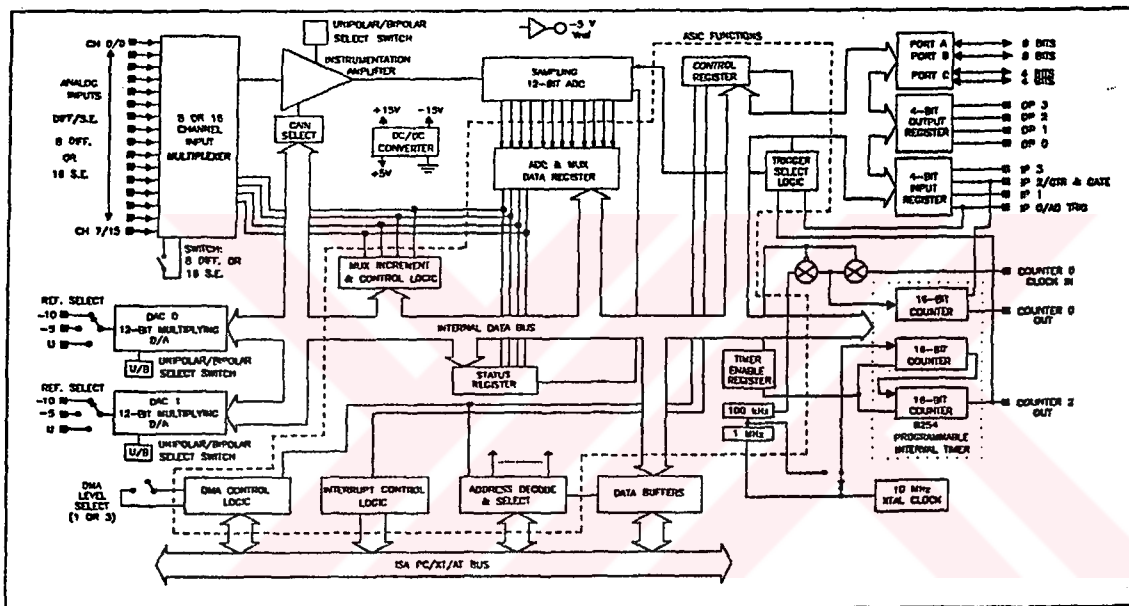


Figure 1-1. DAS-1600 Functional Block Diagram

The DAS-1600 offers 8 differential or 16 single-ended analog inputs with 12-bit resolution at 100 ksamples/sec. You may set the inputs for unipolar (0-10 V) or bipolar (± 10 V) modes, using switches on the Board. Input ranges are software-programmable. The DAS-1601 provides gains of 1, 10, 100 and 500 while the DAS-1602 offers gains of 1, 2, 4, and 8.

Data transfer takes place in one of three ways: by program control, by interrupt service routine, or by DMA. All modes are software-selectable. Demand Mode DMA capability allows full 100 kHz sample rates in both PC/XT and PC/AT computers. This Demand Mode capability allows the DAS-1600 to transfer data at 100 kHz on a PC/AT bus while less sophisticated boards are limited to 70 kHz.

A 3-channel programmable timer (Intel 8254) provides timing for the A/D or can generate output pulses at any rate from 2.5 MHz to 1 pulse/hour. An on-board 10 MHz crystal-controlled oscillator provides the time base. A/D conversions may be triggered three ways: by software command, by the on-board programmable timer, or by an external trigger pulse. The counter timers can also measure frequency, period, and pulse width.

Two 12-bit D/A converter channels are also available. The outputs of these channels have switch-selectable ranges of 0-5, 0-10, ± 5 , and ± 10 V full scale. Regardless of range selected, all analog outputs are set to 0 V at power up. In addition, you may use an external reference to provide analog outputs in other ranges.

Thirty-two bits of digital I/O are available on the DAS-1600. Eight bits of the digital I/O (four input and four output) are on pins of the Main I/O connector. The remaining 24 bits are bi-directional and are on pins of the auxiliary connector. These 24 bits make up two 8-bit ports and two 4-bit ports. Each port may be independently set for input or output. The 24-bit digital port is compatible with the Keithley Metrabyte PIO-12 board. These digital bits may control multiplexers, read external status, gate the counter/timer, etc. Additional features of the DAS-1600 include

- Backward compatibility with the DAS-16G board. Programs for the DAS-16G run on the DAS-1600 without modification.
- Switch-selectable Channel Input Configuration, Base I/O Address, and DMA Level.
- A/D conversion triggering by any of the following: software command, internal programmable-interval timer, or direct external trigger to the A/D. Once the A/D conversion is complete, data transfers may take place via program transfer, interrupt, or DMA.
- A -5 V (± 0.05 V) precision reference voltage output is derived from the ADC reference. Typical applications are providing a DC reference input for the DACs and providing offsets and bridge excitation to user-supplied input circuits.
- A unique burst mode sampling capability can emulate simultaneous sample-and-hold operation.

1.2 DISTRIBUTION SOFTWARE

This manual refers to the DAS-1600 software as the *Distribution Software*. The Distribution Software contains driver files, utility files, example files, and miscellaneous files. Among the miscellaneous files are *FILES.DOC* and *README.DOC*, which are a listing of Distribution Software contents and last-minute software changes, respectively.

Because the Distribution Software arrives in compressed form, it is important that you follow the installation instructions in Chapter 2.

1.3 SPECIFICATIONS

Analog-To-Digital Converter & Front End

- Channels:** 8 differential or 16 single-ended, switch-selectable.
- Resolution:** 12 bits (1 part in 4096 or 244 ppm).
- Absolute Accuracy:** Typical:
0.01% of reading ± 1 LSB, typical for all ranges.

Maximum Error:

For gain less than 500: 0.02% of reading ± 1 LSB max @ 25° C.

For gain = 500: 0.03% of reading ± 1 LSB max @ 25° C.

**Temperature Coefficient
Of Accuracy (includes
ADC):**

Gain:

± 50 ppm/° C for gains of 1, 2, 4, 8, and 10.

± 55 ppm/° C for a gain of 100.

± 60 ppm/° C for a gain of 500.

Offset (Unipolar Ranges):

± 10 μ V/° C ± 5 ppm/° C.

Offset (Bipolar Ranges):

10 μ V/° C ± 10 ppm/° C.

Input Bias Current:

± 40 nA max @ 25° C.

± 60 nA max over operating range.

**Common Mode
Rejection Ratio (DC):**

Gain = 1 74 dB.

Gain = 2 80 dB.

Gain = 4 80 dB.

Gain = 8 86 dB.

Gain = 10 90 dB.

Gain = 100,500 100 dB.

Noise: The following tables show the electrical noise introduced by the analog front end but do not include the uncertainty inherent in the quantization process. The inherent quantization noise introduced by any ADC is due to uncertainty at code boundaries and will add a peak-to-peak value of 1 lsb to the electrical noise and make the rms level 0.5 lsb.

Bipolar (all values are in counts):

GAIN	PK-PK	RMS
1	1	0.1
2	1	0.1
4	1	0.1
8	1	0.1
10	1	0.1
100	2	0.2
500	3	0.5

Unipolar (all values are in counts):

GAIN	PK-PK	RMS
1	1	0.1
2	1	0.1
4	1	0.1
8	1	0.1
10	1	0.1
100	2	0.2
500	3	0.5

Input Overvoltage: ± 35.0 volts continuous.
Throughput: 100 kHz for gains of 1 to 10.
 70 kHz for a gain of 100.
 30 kHz for a gain of 500.

Throughput is the maximum rate at which multiple channels can be scanned and still yield the same result (within ± 1 lsb) as a single channel scan (note that all the channels must be within range of the selected gain to assure proper settling). If using a single channel, use the maximum sampling rate of 100 kHz for gains 100 and greater.

Dynamic Parameters:
Acquisition Time 1.4 μ s.
Aperture Delay 20 ns.
Aperture Uncertainty 300 ps rms.
Conversion Time 8.5 μ s max.

Digital-To-Analog Converter

Resolution: 12 Bits (1 part in 4096 or 244 ppm).

Ranges (Switch Selectable): User Input ± 10 V MDAC Mode.
 0.000 to +5.000 V.
 0.000 to +10 V.
 ± 5.000 V.
 ± 10.00 V.

Linearity: Integral: $\pm 1/2$ lsb typ ± 1 lsb max.
 Differential: ± 1 lsb.
Monotonicity: Guaranteed over operating range.

Output Current Drive: ± 5 mA max.

Gain Accuracy: Adjustable to ± 1 lsb.

Offset Accuracy: Adjustable to zero.

Reference Output Accuracy -5.0 V ± 50 mV.
Voltage Temperature Coefficient ± 30 ppm/ $^{\circ}$ C max.
Load Current ± 5.0 mA max.

DIGITAL I/O (8 Bits On Main 37-Pin D Connector)

OUTPUTS: 4 bits latched-LSTTL levels.

Low Voltage 0.5 V max at $I_{\text{sink}} = 8.0$ mA.

High Voltage 2.4 V min. at $I_{\text{source}} = -0.4$ mA.

INPUTS: 4 bits-LSTTL levels.

Low Voltage 0.8 V max.

Low Current -0.2 mA max.

High Voltage 2.0 V min.

High Current 20 μ A max.

NOTE: TRIG0/IP0 min pulse width = 10.0 ns.

DIGITAL I/O (24 bits On Auxiliary 37-Pin D Connector)

TYPE: NMOS8255A-5

OUTPUTS:

Low Voltage 0.45 V max at $I_{\text{sink}} = 1.7$ mA.

High Voltage 2.4 V min at $I_{\text{source}} = -0.2$ mA.

INPUTS:

Low Voltage 0.8 V max.

Low Current -10 μ A max.

High Voltage 2.0 V min.

High Current 10 μ A max.

PROGRAMMABLE TIMER (3 Down Counters Of 16 Bits Each, 2 permanently Connected To 1/10 MHz)

TYPE: 82C54-2.

OUTPUTS (Buffered): 0.5 V max at $I_{\text{sink}} = 25.0$ mA.

Low Voltage

High Voltage 2.0 V min at $I_{\text{source}} = -15.0$ mA.

INPUTS (Buffered):

Low Voltage 0.8 V max.

Low Current -0.2 mA max.

High Voltage 2.0 V min

High Current 20 μ A max.

Power Supply Requirements:

+5 VDC, 800 mA.
+12 VDC, 40 mA.

Environmental

Operating Temperature: 0 to 70° C

Storage Temperature: -20 to 70° C

Humidity: 0 to 95% non-condensing

1.4 ORDERING INFORMATION

- DAS-1601** This package includes the DAS-1601 (features software programmable gains of 1, 10, 100, and 500) and standard software package. The standard software package contains installation and configuration software, the Pop Up Control Panel and Call Command Interface Support for BASIC, Quick BASIC, and QBASIC. Documentation is also provided.
- DAS-1602** This package includes the DAS-1602 (features software programmable gains of 1, 2, 4 and 8) and standard software package. The standard software package contains installation and configuration software, the Pop Up Control Panel and Call Command Interface Support for BASIC, Quick BASIC, and QBASIC. Documentation is also provided.
- ASO-1600** Advanced Software Option for the DAS-1601/16-2. This includes Call Command Interface support for C and Pascal, the Dynamic Link Library, and the File I/O Command Interface. Documentation is also provided.
- C-1800** Cable for connecting DAS-1600 to a STA-1600.
- STA-16** Screw Terminal Adapter Board. Refer to Chapter 2 for connections.
- STA-U** Universal Screw Terminal Adapter Board.
- STC-37** Direct DAS-1600 to screw terminal interface. Refer to diagram on STC-37 cover for connections.
- EXP-16** 16 channel expansion multiplexer and signal conditioning board. Requires S-1600 cable and the PG-408 option. Refer to the EXP-16 user guide for usage information.
- EXP-GP** 8 channel signal conditioning board with Wheatstone bridge and RTD interface. Requires S-1600 cable. Refer to the EXP-GP user guide for usage information.
- MB-Series** Signal Conditioning Modules. Refer to the MB-Series user guide for usage information.

ISO-4	4 channel isolated expansion multiplexer.
ASYST 1, 2, 3, 4 *, **	Data Acquisition and Analysis programming language.
EASYEST LX *, **	Single-screen, icon-based data acquisition, analysis, and graphical display software.
EASYEST AG *, **	Single-screen, icon-based data acquisition, analysis, and graphical display software.
VIEWDAC *, **	Data Acquisition, analysis, and graphical display software.
SNAP-MASTER	Menu-driven Data Acquisition and Analysis package from H.E.M. Data Corporation.
LABTECH NOTEBOOK	Menu-driven data acquisition and analysis from Laboratory Technologies Corporation.
STREAMER	Menu-driven Data Acquisition package which allows data to be written to a hard disk at up to 100Khz.
SSH-4/A	Refer to the SSH-4/A user guide for usage information.

* You must use the DAS-1600 driver supplied with this optional package. Do not use the Keithley MetraByte Drivers.

** Support pending. Contact manufacturer for availability.

■ ■ ■

INSPECTION, CONFIGURATION, & INSTALLATION

2.1 INSPECTION

After removing the wrapped Board (DAS-1600) from its outer shipping carton, proceed as follows:

1. Before unwrapping the Board, hold it in one hand while placing the other firmly on a metal portion of the computer chassis (the computer must be turned Off but grounded) to discharge any static electricity.
2. Carefully remove the Board from its anti-static wrapping material. You may wish to store the wrapping material for possible future use.
3. Inspect the Board for signs of damage. If any damage is apparent, arrange to return the Board to the factory (see the chapter entitled *Instructions For Factory Returns*).
4. Check the remaining contents of your package against the packing list to be sure your order is complete. Report any missing items to the factory, immediately.
5. When you are satisfied with the inspection, you are ready to configure the Board. Refer to the next section for configuration options.

2.2 CONFIGURATION OPTIONS

Switches & Jumpers

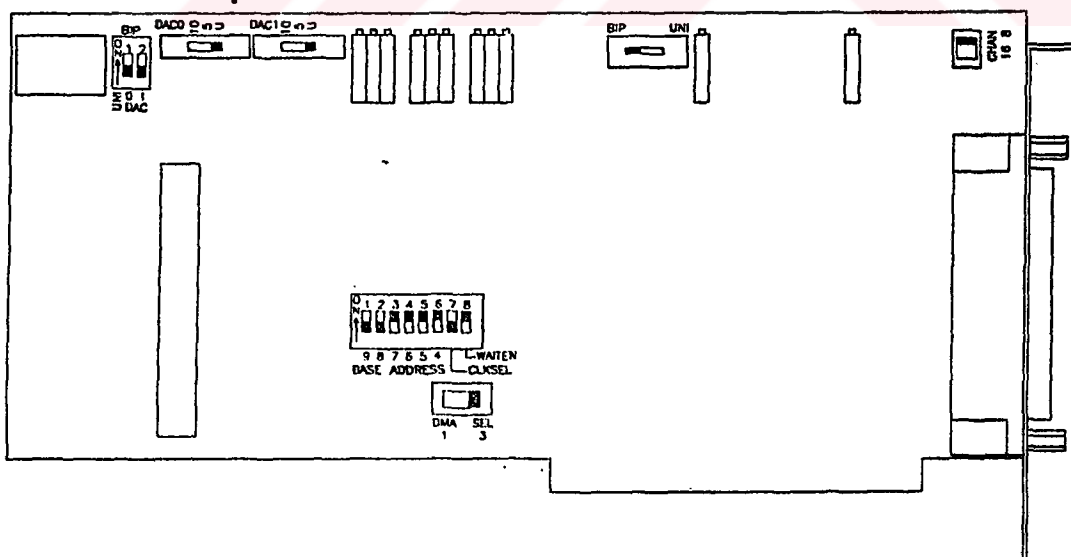


Figure 2-1. DAS-1600 Configuration Switch Locations.

DAC Bipolar/Unipolar Switch

A 2-section DIP switch sets DAC 0 and DAC 1 for Unipolar or Bipolar. The left section (labeled 0) is for DAC 0, the right (labeled 1) for DAC 1. Switch either section up for Bipolar, down for Unipolar (the default is Bipolar). Refer to the chapter entitled *Applications* for more information.

DAC0 & DAC1 Switch

Two 3-position switches offering 10, 5, and U selections. When DAC 0 and/or DAC 1 is set for Bipolar, the 10 and 5 positions output ± 10 V and ± 5 V, respectively (the default setting is 5, for Bipolar). When DAC 0 and/or DAC 1 is set for Unipolar, the 10 and 5 positions output 0-10 V and 0-5 V, respectively. The U position on both switches sets the User Input Multiplying Mode. Refer to the chapter entitled *Applications* for more information.

ADC Bipolar/Unipolar Switch

A 2-position slide switch sets A/D operation to Bipolar or Unipolar. The default setting is Bipolar/

Chan 8/16 Switch

A 2-position slide switch configures the A/D inputs as 8 differential or 16 single-ended inputs. The default setting is 8 differential.

DMA Channel Select Switch

A 2-position slide switch selects DMA Channel 1 or 3. The default setting is 3.

Base Address/Clock Select/Wait Enable Switches

A single, 8-position DIP switch accommodates the Base Address, the Clock Select, and the Wait State Enable parameters as shown in Figure 2-2. The default settings are Base Address = 768 (300h), Wait State is Off (Up), and Clock Select is 10 MHz (Down).

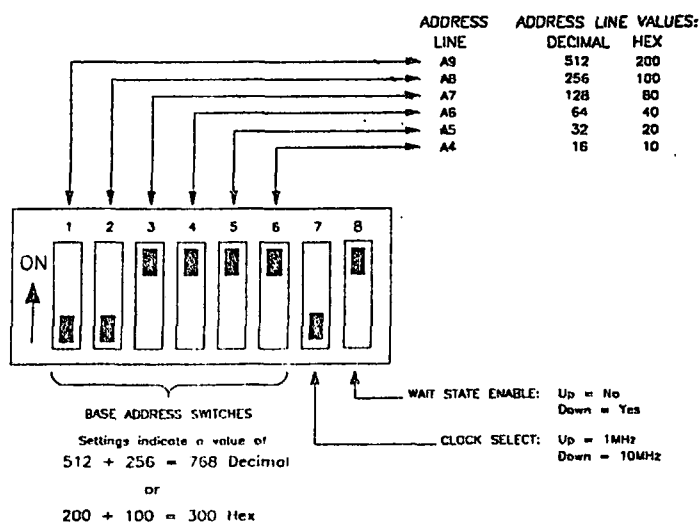


Figure 2-2. Settings for Base Address, Clock Select, and Wait State Enable.

Jumper J4

The position of this jumper determines whether the external trigger for IP0/TRG0 arrives via Pin 2 or Pin 8 of Connector J3. Placing the jumper on the left two pins links Pin 2; the right two pins link Pin 8. The default position is the left two pins.

2.3 MAIN I/O CONNECTOR

Analog and digital I/Os use a 37-pin, D-type connector that projects through the connector panel at the rear of the computer. The mating connector is a standard, 37-pin D-type female such as an ITT/Cannon #DC-37S for soldered connections. Insulation displacement (flat cable) types are readily available (for example, Amp #745242-1). Other manufacturers make equivalent parts.

Pins 11 through 18 perform a double function, depending on the setting of the Channel Configuration switch. In 8-channel differential configuration, these pins provide the low inputs of Channels 0-7 corresponding to the high inputs of these channels on pins 30-37. In 16-channel single-ended configuration, they provide additional channel-high inputs for Channels 8-15. Figure 2-3 depicts the I/O connector and its signal connections.

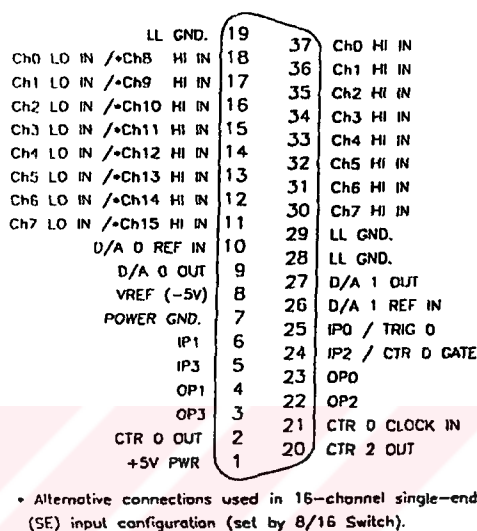


Figure 2-3. Rear View of I/O Connector.

2.4 SOFTWARE INSTALLATION

Backing Up The Distribution Software

As soon as possible, make a back-up copy of your Distribution Software. With one (or more, as needed) formatted diskettes on hand, place the Distribution Software diskette in the A Drive of your PC and log to that drive by typing **A: .** Then, make your back-up copy using the DOS **COPY** or **DISKCOPY** command (see your DOS reference manual). **DISKCOPY** is the better choice because it copies diskette identification as well as Distribution Software.

Installing The Distribution Software

Your Distribution Software is usable only after installation on the hard drive of your PC. For installation, insert the Distribution Software diskette (Diskette #1) in the A Drive, and type **INSTALL <Enter>**. Follow the instructions on the screen. The **INSTALL** program automatically loads the Distribution Software into the directory DAS1600 on your C drive.

Distribution Software Contents

Your Distribution Software contains the ASCII file *FILES.DOC*, which lists and describes all the other Distribution Software files. *FILES.DOC* is readable with any text editor (word processor) or with the DOS *TYPE* command. To learn of last-minute changes, be sure to read the ASCII file *README.DOC*.

2.5 THE CONFIGURATION PROGRAM

To facilitate the configuration of your DAS-1600, the Distribution Software includes *D1600CFG.EXE*. This program presents the board's configuration choices in menu form. After making your selections from the menu, you have the option of switching to a diagram of the corresponding switch settings to use as a reference for setting up your Board. The file you create with this utility may see later use in applications programs (via the Call *DAS1600DevOpen*) and/or while loading the driver for the Pop-Up Interface (via the */F = filename* switch for *MDAS1600.EXE*).

Start the *D1600CFG.EXE* program by typing **CONF1600 *filename***, where *filename* is the name of the reference file for your settings. The *filename* you choose may be a file you wish to create, or it may be an existing file you wish to read or change. Keithley Metrabyte provides a file *DAS1600.CFG* which configures the DAS-1600 for the factory defaults.

Default Configuration File (DAS1600.CFG) Settings

The DAS1600.CFG is set for the following:

Board:	0
Name:	DAS1602
Base Address:	768 (300h)
DMA Channel:	3
DAC0 Reference:	5 V
DAC1 Reference:	5 V
DAC0 Polarity:	Bipolar
DAC1 Polarity:	Bipolar
Clock:	10 MHz
Wait State:	Off
Interrupt Level:	7
A/D Channel Mode:	Bipolar
A/D Channel Config.:	Differential
# of EXP-16:	0
# of EXP-GP:	0
Port A:	Input
Port B:	Input
Port CL:	Input
Port CH:	Input

Suppose you wish to create a file *MY1600.CFG* to store a new set of configuration settings; type **CONF1600 MY1600.CFG**. If this file already exists and you wish to read and/or change it, you must still type **CONF1600 MY1600.CFG**. In either case, the opening screen will be the same: a blank menu screen with the name of your reference file beneath the screen header. To move from the opening screen, you must enter a 1 or 2 for the number of DAS-

1600 boards you plan to configure. The next screen contains the menu of switch-controlled parameters. The upper-left corner of the menu box shows the number of the Board to be configured (to change this number, press **N**).

DAS-1600/1400 Configuration			
SWITCH SETTINGS			
[Board #] S1			
<div>1 2 3 4 5 6 C H</div> <div>BASE ADDRESS</div>	<div>SS 1 3</div> <div>DMA SEL</div>	<div>S2 UN1 BIP</div> <div>A/D Mode</div>	<div>S3 16 8</div> <div>A/D Config</div>
<div>S8 BIP 1 2</div> <div>DAC</div>	<div>10 5 U</div> <div>DAC0 Ref</div>	<div>10 5 U</div> <div>DAC1 Ref</div>	
[Commands/Status] Press any key to return to main screen. . .			

Figure 2-4. Switch settings display.

To select and modify one of the parameters, follow the instructions in the *Commands/Status* box (bottom of screen). Note that these instructions vary with parameters.

After completing your parameter modifications, press **S** to see the display of corresponding switch settings (see Figure 2-4). Use this display as a reference for setting your Board switches.

When you exit the D1600CFG.EXE program, you are asked whether to save the settings you have selected. Pressing **Y** saves an ASCII record of your settings in the reference file (MY1600.CFG, in this example). You may recall and modify this file at a later time.

2.6 BOARD INSTALLATION

WARNING!

ANY ATTEMPT TO INSERT OR REMOVE ANY ADAPTER BOARD WITH COMPUTER POWER ON COULD DAMAGE YOUR COMPUTER!

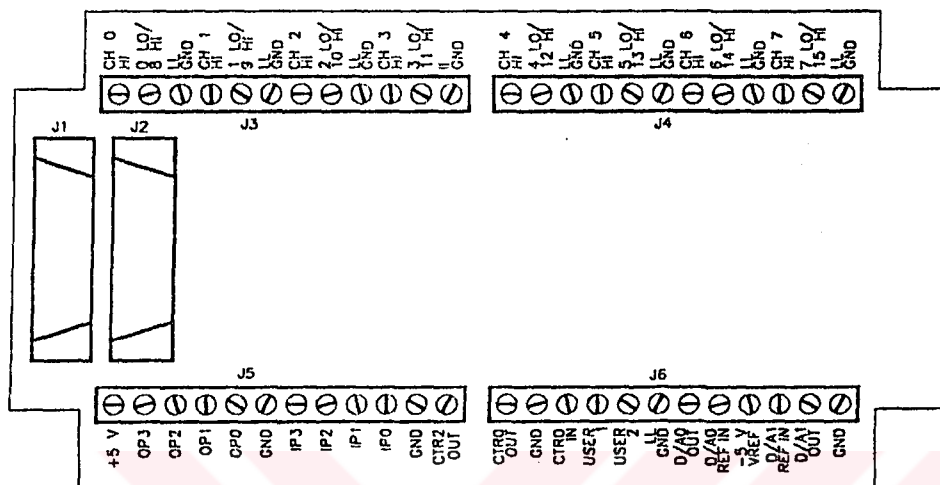
To install the Board in a PC, proceed as follows:

1. Turn Off power to the PC and all attached equipment.
2. Remove the PC chassis cover.
3. Select an available option slot. Loosen and remove the screw at the top of the blank adapter plate, then slide the plate up and out to remove.
4. Be sure the board switches have been properly set (refer to the preceding section).
5. Insert and secure the board connector in the selected accessory slot.

6. Replace the PC cover.
7. Plug in all cords and cables. Return power to the computer.

You are now ready to make any necessary system connections, install the DAS-1600 software, and perform calibration and perform checks on calibration and adjustment.

2.7 STA-16 CONNECTIONS



3A 3B 3C

METHODS OF CONTROL

3.1 GENERAL

The DAS-1600 Standard Software Package provides the following options:

- The Pop Up Control Panel
- The Call Driver for BASIC
- Low-level-Register I/O Programming

Additional programming options, PASCAL and C support, and Windows 3.X language support are available in the Advanced Software Option (ASO-1600; see *Ordering Information*, in Chapter 1).

3.2 THE POP UP CONTROL PANEL

The Pop Up Control Panel allows direct control of DAS-1600 operation, without programming requirements. You may configure the board to perform an analog or digital operation and to store the resultant data in a disk file. The Pop Up uses four control panels that you may "pop up" (bring to the screen) with keyboard while under DOS control or inside an applications program. This Interface provides a quick way to test your board as well as to debug/monitor your operation. Chapter 5 discusses Pop Up Control Panel operation.

NOTE: The Pop Up Control Panel does not support the use of EXP-GP or EXP-16 boards with the DAS-1600.

3.3 THE CALL DRIVER

The Call Driver is a collection of functions (Calls) performing the most commonly used setup and operating functions in data acquisition applications. You may incorporate these Calls in application programs you write in Interpreted BASIC, QuickBASIC, or QBASIC. The Calls preclude the need for any register-level programming for the functions they perform.

Chapter 6 lists and briefly describes each of the Call drivers and each of the Calls. Chapter 7 covers the use of each Call and provides examples in Interpreted BASIC, QuickBASIC, and QBASIC.

3.4 REGISTER-LEVEL I/O PROGRAMMING

You may also program the DAS-1600 at a basic level by writing directly to the on-board registers. Register-level programming requires an understanding of PC architecture, PC Peripheral Controllers (the 8259 Interrupt Controller, the 8237 DMA Controller, etc.), and the

DAS-1600 hardware. While most languages are suitable for this programming, BASIC is not recommended because its lack of interrupt or DMA processing functions does not support background data-acquisition tasks such as Interrupt and DMA driven applications.

Chapter 8 supplies DAS-1600 register maps and corresponding bit functions.

■ ■ ■



VIBROMETER 20

**Vibration Severity Measuring Instrument
in Accordance with ISO 2954 and DIN 45666**



**Functional Description
Operation
Application**

1. Introduction

1.1 Application and Functional Description

The vibration severity measuring instrument VIBROMETER 20 is a battery operated, portable vibration measuring instrument. It is in compliance with standards ISO 2954 and DIN 45666 for vibration severity measuring instruments and can be used for comparison-, test-, and acceptance measurements on:

- electric motors and generators
- turbines and compressors
- pumps
- centrifuges and separators
- blowers and fans
- machinery, etc.

The electrodynamic vibration velocity pickup VS-080 or T 77 is part of the standard equipment. The pickup, with its pickup probe, is held by hand against the machine to be tested. The pickup can also be attached by means of a mounting magnet which is also part of the delivery.

The vibration velocity with units mm/s or inch/s or the vibration displacement in μm or mils can be selected as measuring parameter.

The instruments indicate the measured value as digital readout. A "steady" key (key with snail symbol) will steady the digital display when there is a strongly fluctuating measuring value. In the LCD display the selected unit of measure is displayed in addition to the measured value. When the batteries are weak or with empty rechargeable batteries the remark "BAT" is displayed.

VIBROMETER 20 permits the conducting of vibration measuring in the frequency range of 10 ... 1000 Hz (600 ... 60000 rpm) in accordance with ISO 2954 and DIN 45666. In order to obtain low frequency vibrations, as they occur with slowly running machines, measurements can be taken in the frequency ranges 3 ... 300 Hz (180 ... 18000 rpm) and 3 ... 1000 Hz (180 ... 60000 rpm).

For recording the measured values on a recorder and for displaying the vibrations on an oscilloscope, output sockets are present, where the filtered signal and a direct voltage signal which is proportional to the preselected measuring parameter are supplied.

1.2 Standards

The measuring instrument VIBROMETER 20 meets all requirements of the following standards and guidelines:

- VDI Guideline 2056: "Evaluation criteria for mechanical vibration of machines"
- ISO Standard 2372: "Mechanical vibrations of machines with operating speeds from 10 to 200 rev/s"

- British Standard 4675; 1971: "A basis for comparative evaluation of vibration in machinery"
- AFNOR E90–300: "Mechanical vibrations of machines with operating speeds from 10 to 200 rpm"

While the above regulations pertain to the entire machine industry, the following standards are limited to the vibration severity measuring of electric motors and generators:

- DIN – ISO – Standard 2373: "Mechanical vibrations of rotating electrical machines with shaft heights between 80 and 400 mm"

For the manufacturers and operators of large rotating machines measuring details are set down in:

- ISO Standard 3945: "Mechanical vibration of large rotating machines with speed range from 10 to 200 rev/s"

The above-mentioned standards and guidelines recommend to the user limit values for the evaluation of machine vibrations. By comparing the measured vibration severity with the specified limit values, the vibration behaviour of a machine can immediately be categorized into ranges of "good", "satisfactory", "still acceptable" or "unacceptable".

To ensure that the manufacturer as well as the customer obtain equal and reproducible measuring values, the technical properties of vibration severity measuring instruments are defined in special standards:

- DIN 45666: "Vibration severity measuring instrument"
- ISO Standard 2954: "Requirements for an instrument for measuring vibration severity in rotating and reciprocating machinery"

2. Extent of delivery and accessories

The vibration severity measuring instrument VIBROMETER 20 consists of a display unit and vibration pickup, which are both placed into an attache case.

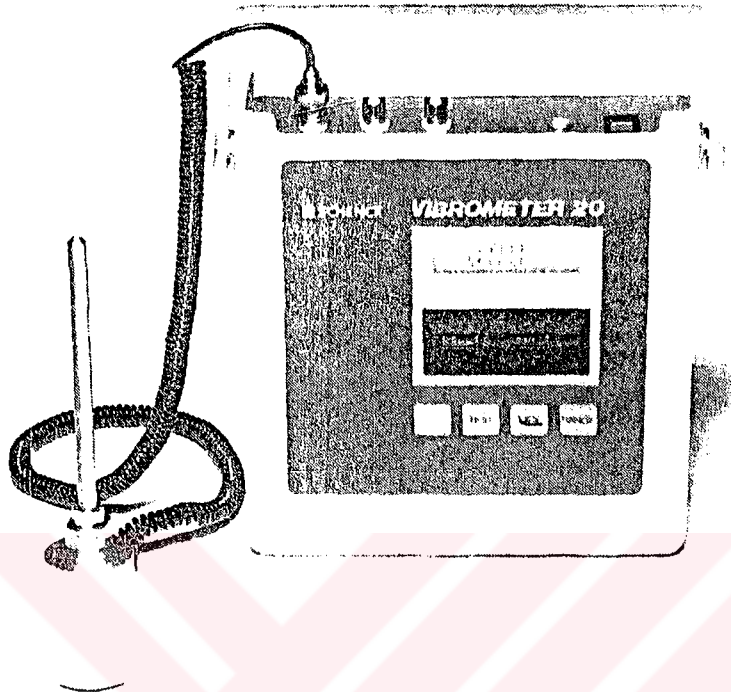


Fig. 1: Vibration Severity Measuring Instrument VIBROMETER 20

90359

Standard Equipment:

- 1 Indication instrument VIBROMETER 20 with two zinc-carbon drycell batteries (9.0 V block per IEC [6F22])
- 1 Absolute vibration pickup VS-080 or T 77 with magnetic base, pointed straight probe and 5 m measuring cable
- 2 Operating instructions in the German, English, and French language
- 1 Attache case for transporting the instrument, the standard accessories and option 01.

Option 01 – 1

Rechargeable nickel-cadmium batteries (9.0V block, 100mAh; IEC [6F22]) with charger.

The drycell batteries contained in the standard delivery are replaced by rechargeable NiCd batteries.

The charging of the NiCd batteries and the use of the external power supply is made possible by the charger which is included in the delivery.

Extent of Delivery:

- 2 Rechargeable NiCd batteries
- 1 Charger unit for external power supply 220/110V \pm 10%, 50 . . . 60 Hz or with line plug per American standard for 117 V \pm 10%, 50 . . . 60 Hz

Option 02

Additional absolute vibration pickup VS-080 or T 77

Extent of Delivery:

- 1 Absolute vibration pickup VS-080 or T 77 with mounting magnet, straight probe and 5 m measuring cable

Option 03

Additional extension cable.

for vibration pickup VS-080, with connection plug and intermediate plug (max. admissible length 200 m)

Option 03—1: 1 extension cable 20 m long

Option 03—2: 1 extension cable 5 m long

Option 04

Spare Parts Kit

The spare parts kit is especially intended for the export of the instrument and essentially contains components (specific integrated circuits and similar items).

Option 04—1: Spare parts kit for VIBROMETER 20 with drycell battery operation

Option 04—2: Spare parts kit for VIBROMETER 20 with rechargeable NiCd batteries

Option 05

Oscilloscope

For displaying the waveform of vibrations.

Extent of Delivery:

- 1 10 MHz dual beam oscilloscope with time base, X-Y operation and screen area 80 \times 100 mm
- 1 Connection cable to the VIBROMETER, 2 m long

Mass: 8.0 kg

3. Technical Data

3.1 Technical Data of the Pickup

Type:	VS-080 or T 77
Measuring parameter:	Vibration velocity
Measuring principle:	Electrodynamic
Measuring direction:	Horizontal to vertical according to sketch

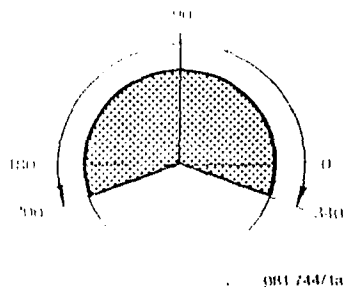


Fig. 2: Measuring direction of the pickup

Sensitivity:	72 mV/mm/s (AC) $\pm 2\%$ at ($R_L = 100\text{ k Ohm}$)
Internal impedance:	$R_i = \text{approx. } 2.8\text{ k Ohm}$
Minimal load impedance:	$R_L = 50\text{ k Ohm}$
Natural frequency:	$f_0 = 15\text{ Hz} \pm 0.3\text{ Hz}$
Operating frequency range: ($\pm 3\text{ dB}$ – points, see Addendum)	
– without frequency response linearization:	20 ... 2000 Hz
– with frequency response linearization (part of VIBROMETER 20):	2 ... 2000 Hz
Max. admissible vibration displacement:	$s_m = \pm 1\text{ mm}^*$
Operating temperature range:	$-34 \dots +100^\circ\text{C}$
Mounting bore:	M8 (depth: 10 mm)
Protective housing:	IP 65
Electric connection cable:	1 core, shielded
Cable length:	Approx. 5 m

*) Below the natural frequency f_0 the measurable vibration displacement s_{mf1} increases. It is calculated according to the relationship: $s_{mf1} = s_m \cdot [f_0/f_1]^2$

Special properties:	Stainless steel housing, pickup element hermetically sealed
Mass (without cable):	Approx. 0.35 kg

3.2 Technical Data of the Vibration Severity Measuring Instrument VIBROMETER 20

Type:	Portable vibration severity measuring instrument in accordance with ISO 2954 and DIN 45666
Frequency Range:	10 ... 1000 Hz (600 ... 60 000 rpm) (Frequency response, see Addendum) switchable to 3 ... 1000 Hz (180 ... 60 000 rpm) 3 ... 300 Hz (180 ... 18 000 rpm)
Display Unit:	3½ digit LCD readout for vibration velocity and vibration displacement and display of the measur- ing parameter <ul style="list-style-type: none"> – measuring value – unit of measure – dead battery "BAT" – function test indication
Measuring Parameters:	<ul style="list-style-type: none"> – Effective value of the vibration velocity in mm/s and inch/s* – Peak-to-peak value of the vibration displace- ment s in μm▲ and in mils♦* – Peak value of the vibration displacement in μm▲
Measuring Ranges:	0.01 ... 199.9 mm/s 0.1 ... 1999 μm 0.1 ... 19.99 inch/s* 0.01 ... 199.9 mils* The measuring ranges are decade switchable in two ranges.
Measuring Error:	Within ISO 2954 and DIN 4566. Deviation of the transfer factor of pickup and measuring instrument smaller than $\pm 10\%$ of the reference value at 80 Hz in the frequency range 10 ... 1000 Hz.

*) 1 inch = 25.4 mm
1 mil = 1/1000 inch = 25.4 μm
1 inch/s = 25.4 mm/s

Connection for Oscilloscope
and Alternating
Voltage Recorder

Alternating voltage $0 \dots 1V_{\text{rms}}$
at $R_i \text{ min} = 10 \text{ k Ohm}$

Direct Voltage Connections
for X-Y Recorder:

Direct voltage $0 \dots 2V$
at $R_i \text{ min} = 10 \text{ k Ohm}$

Power Supply

1. External (line) Operation with Charger:

$220/110V \pm 10\%$, $50 \dots 60 \text{ Hz}$ or $117V$
 $\pm 10\%$, $50 \dots 60 \text{ Hz}$ with line plug per
American standard

2. Battery Operation:

Two zinc-carbon drycell batteries
(9.0V block per IEC [6F22]).
Operating time approx. 120 hours

3. Charger Operation:

Two rechargeable NiCd batteries (9.0V block per
IEC [6F22]). For example: Option 01-1.
Operating time approx. 80 hours, charging time
approx. 14 hours

Operating Temperature
Range:

$0 \dots +60^\circ\text{C}$

Storage Temperature:
Range:

$20 \dots +90^\circ\text{C}$

$20 \dots +60^\circ\text{C}$ with battery

Dimensions:

Indication instrument: $200 \times 60 \times 220 \text{ mm}$.
Attache case with indication instrument and
accessories: $410 \times 110 \times 310 \text{ mm}$

Mass:

Indication instrument: 1.3 kg.
Attache case with indication unit and accessories:
3,8 kg

4. Operating elements and their function

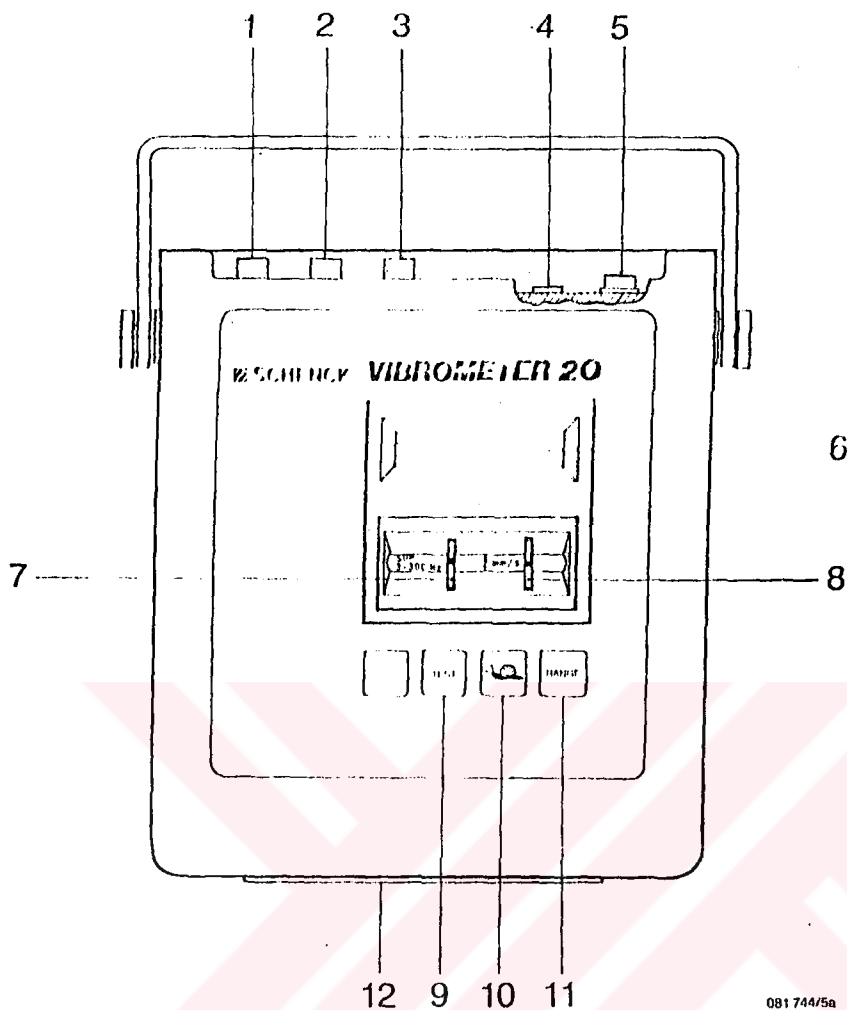


Fig. 3: Operating Elements

- 1: **BNC input socket "C1"** for pickup VS-080 or T 77.
- 2: **BNC output socket "C2"** supplies a **readout value** proportional **alternating voltage** signal. $V_{rms} = 1V$ at "C2" corresponds to the measuring range limit value 1999 (in digits).
- 3: **BNC output socket "C3"** supplies a **readout value** proportional **direct current** signal. 2V at "C3" corresponds to the measuring range limit value 1999 (in digits).
- 4: **Flange socket "C5"** for line connection and recharging with charger operation (Option 01 - 1).

- 5: **ON/OFF switch "C6"**.
- 6: **The LCD readout unit** displays the measured value. Switchable to vibration velocity and vibration displacement. In addition, the LCD readout unit indicates the unit of the measuring parameter, the indication "BAT" for weak batteries.
- 7: **Measuring range selector switch** – (left drum) for switching to the desired frequency range of wide band measuring (SUM ...).
Possible measuring steps are:
SUM 10 ... 1000 Hz
SUM 3 ... 1000 Hz
SUM 3 ... 300 Hz
- 8: **Measuring parameter selector switch** (right drum) switchable to vibration velocity (in mm/s or inch/s) and vibration displacement (in μm^Δ , μm^∇ , and mils $^\Delta$).
- 9: **TEST key** for checking the operational capability of the instrument (see Section 5.2).
- 10: **The "Steady" key** – symbolized by a snail – allows for a steadying of the digital display value when there is a strongly fluctuating measuring value.
- 11: **The RANGE key** – for switching the measuring sensitivity. A brief depressing of the Range key changes the measuring sensitivity by a factor of 10 (the decimal point alternates in jumping one position to the left or to the right).
- 12: **Battery compartment**

5. Start-up

5.1 Power Supply

The instrument can be operated in three ways:

- a) Battery operation with two drycell batteries 9V per IEC (6F22)
- b) Charger operation with two rechargeable NiCd batteries (9.0V, 100 mAh, per IEC [6F22])
- c) Line operation 220/110V \pm 10%, 50 ... 60 Hz or 117 V \pm 10%, 50 ... 60 Hz with line plug per U.S. standard

To a): **Battery Operation**

With dead batteries, "BAT" is displayed on the LCD readout unit. Switch off the instrument before inserting or replacing the batteries.

The four screws at the cover of the battery compartment must be removed when inserting or replacing the batteries.

NOTE:

Drycell batteries cannot be recharged. They must be removed with external power supply operation – otherwise there is DANGER OF EXPLOSION.

IMPORTANT:

Remove dead batteries immediately. Replace both batteries of the set of batteries **at the same time** with fresh batteries. Use only the same type of batteries.

To b): **Charger Operation (Simultaneous operation using outside power supply with charging unit is possible)**

When using rechargeable NiCd batteries IEC (6F22), please note the following:

Switch off instrument before inserting batteries. Prior to initial operation, charge batteries for 14 hours. Avoid operation with discharged batteries. Recharge at proper time.

With dead batteries, "BAT" is displayed in the LCD readout unit.

To c): **External Power Supply with Charger**

The VIBROMETER 20 can be operated with the charging unit without batteries.

NOTE:

Drycell batteries cannot be recharged. They must be removed when using external power supply – DANGER OF EXPLOSION.

5.2 Function Test

The TEST key is used for checking all VIBROMETER 20 functions. All function elements or function units of the instrument are tested.

With the instrument switched on and TEST key depressed, the test value relevant to the measuring mode and measuring parameter is displayed on the LCD display (see table). In general, it is sufficient to test the instrument in position SUM 10 ... 1000 Hz (left drum) and unit "mm/s" (right drum).

Measuring Range	Measuring Parameter and Tolerance Range				
	mm/s	μm^{\wedge}	$\mu\text{m}^{\blacktriangledown}$	inch/s	mil $^{\blacktriangledown}$
Tolerance in %	± 5	± 5	± 5	± 5	± 5
SUM 10 ... 1000 Hz	9.5.0 10.5.0	9.5 10.5	19.0 21.0	.3.73 .4.13	0.7.5 0.8.3
SUM 3 ... 1000 Hz	9.4.8 10.4.8	9.5 10.5	19.0 21.0	.3.73 .4.13	0.7.5 0.8.3
SUM 3 ... 300 Hz	9.0.4 10.0.4	9.6 10.6	19.3 21.3	.3.54 .3.94	0.7.6 0.8.4

Table 1: Tolerances with Function Test (relative to measuring range and measuring unit)

5.3 Attaching the Vibration Pickup to the Machine

The pickup is to be attached to the machine to be evaluated so that its center axis meets the rotor axis at right angles. The measuring direction, however, as given in the sketch, is as desired in the specified angular area.

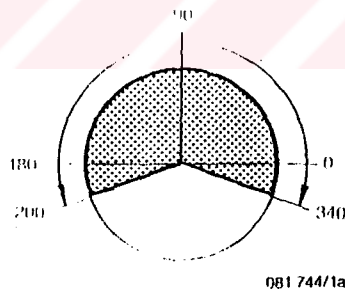


Fig. 4: Measuring Directions

As an ideal mounting location, a location on the bearing bushing is to be selected. If this cannot be done in practice, a location near the bearing bushing should be selected which supplies direct information about the bearing vibration.

However, the vibration pickup should not be attached to parts which themselves could become resonant, for example, metal enclosures, pipes.

If the exact position of the pickup is not readily determined, then measurements should first be made, to obtain the location and the angular position of the maximum vibration at a functionally important location.

The pickup mass, oscillating in resonance, is approximately 0.35 kg. Therefore, the pickup can be used for checking machines with a total co-vibrating mass of (inclusive rotor, machine frame, covering, etc.) more than 4 kg.

Generally, the pickup is held by hand against the measuring location. The probe is to be inserted into the pickup.

At measuring locations consisting of ferromagnetic material, the pickup can be mounted with the supplied holding magnet. The mounting surface should be clean and smooth.

In case of measurements at non-magnetic or uneven locations that require more time, it is recommended to screw the pickup to the measuring location with a stud screw (M8). The screw can be glued to the machine with suitable metal glue.

The pickup connection on the VIBROMETER 20 is at the input socket "C1".



6. Measuring tasks

The ISO Standard 2954 and the DIN Standard 45666 demand a measuring and a combining of all mechanical vibrations occurring in the frequency range of 10 ... 1000 Hz.

In addition to this, VIBROMETER 20 offers the possibility to measure low frequency vibrations selectivity in the frequency range 3 ... 300 Hz or 3 ... 1000 Hz.

For recording the measured values and for displaying the wave forms, connection sockets are provided for the recorder and/or the oscilloscope.

6.1 Measuring of the Effective Value of the Vibration Velocity

The effective vibration velocity of all partial vibrations of a vibration mixture can be measured in three frequency ranges:

- a) SUM 10 ... 1000 Hz – Standard measuring range for vibration **severity**
 - b) SUM 3 ... 300 Hz
 - c) SUM 3 ... 1000 Hz
- } – Special measuring ranges

To a): **Standard measuring range 10 ... 1000 Hz**

Vibration severity measuring in accordance with VDI-2056, ISO 2372, BS4675, and AFNOR E90–300.

The vibration **severity** is defined as the largest **effective value of the vibration velocity in the frequency range SUM 10 ... 1000 Hz** occurring at a functionally important location of a machine (for example: bearing).

To b): **Special Measuring Range 3 ... 300 Hz**

This special range is intended for low speed machines (speed range 180 ... 600 rpm) where higher frequency components of the vibration velocity are not to be considered.

To c): **Special Measuring Range 3 ... 1000 Hz**

This special range is intended for low speed machines where the higher frequency components of the vibration velocity are to be taken into account.

6.1.1 Sequence of the Vibration Velocity Measuring

Function Test:

- See rear panel of the instrument. For a detailed function test of the measuring instrument see Section 5.2.

Connection of Accessories:

- Connect the pickup to the VIBROMETER 20 at socket "C1"
- Attach the pickup to the machine when the measuring takes longer. See Section 5.3.

Setting of the Display Unit:

- Switch "C5" in position "ON"
- Measuring mode selector switch (left drum) in position SUM 10 ... 1000 Hz*
- Measuring parameter selector switch (right drum) in position mm/s or inch/s (depends whether readout is to be in metric units or inch units).

Measuring:

- To measure, the pickup is held by hand against the machine to be tested. The measuring instrument immediately indicates the effective value of the vibration velocity.

Measured Value Readout:

- The measured value can be read from the LCD readout unit. If needed, change the sensitivity by 10 by quickly depressing the RANGE key.

Recording the Measured Values:

- The measured values can be recorded on the enclosed Form SMII (see Addendum). See Section 6.1.6 for an example.

6.1.2 Connection of Recorder and Oscilloscope

For recording or displaying the mechanical vibrations, commercial recorders and measuring instruments can be connected to the output sockets "C2" and "C3" of the VIBROMETER 20.

The following signals are supplied at the sockets:

Socket "C2"

Alternating voltage proportional to the filtered measuring signal.

Voltage: $U = 0 \dots 1V_{rms}$

Transfer Factor: 1V corresponds to the measuring range limit value of the digital indication.

Load Impedance: $R_l \text{ min } = 10 \text{ k Ohm}$

Socket "C3"

Direct voltage proportional to the amount of the preselected measuring parameter.

Voltage: $U = 0 \dots 2 \text{ V}$

Transfer Factor: 2V correspond to the measuring range limit value of the digital indication.

Load Impedance: $R_l \text{ min } = 10 \text{ k Ohm}$

* The vibration **severity** is measured in this position, see Section 6.1.

6.1.3 Evaluation of the Measured Results

The evaluation can proceed according to the empirical values listed in Section 6.1.4 and 6.1.5 which are taken from the VDI Guideline 2056, the ISO Standard 2372, DIN 45666, and the British and French Standards already mentioned in Section 1.2.

6.1.4 Evaluation Criteria According to VDI Guideline 2056 and ISO Standard 2372

First, the machine that is to be tested is to be placed in one of the defined machine categories (see also Table 2). Then, for the appropriate machine group the evaluation limits for the levels "good", "satisfactory", "still acceptable", and "unacceptable" can be taken from the corresponding table. The limit values are to be compared with the vibration **severity** (i.e. the largest effective value of the vibration velocity at a functionally important machine location).

Definition of the Machine Groups

Group K:

Individual drive parts of prime movers and driven-machines, which, when in operation, are permanently connected to the machine as a whole, especially mass produced electric motors up to approximately 15 kW.

Group M:

Medium-sized machines, especially electric motors of 15 to 75 kW without special foundations; also permanently installed drive parts and machines (up to approximately 300 kW) having only rotating parts and mounted on special foundations.

Group G:

Machines installed on high-tuned, rigid or heavy foundations, large prime movers and driven machines having rotating masses only.

Group T:

Large prime movers and driven machines with only rotating masses installed on low-tuned foundations, for example turbo machinery, especially those having foundations designed in accordance with lightweight construction principles.

Group D:

Machines and prime movers having mass effects that cannot be compensated, installed on high-tuned ("rigidly supported") foundations.

Group S:

Machines and prime movers with mass effects which cannot be compensated and installed on low-tuned ("flexibly supported") foundations; also machines with rotat-

ing, loosely attached masses, such as beater shafts of mills and finally machines having varying unbalances which cannot be compensated, these machines can function free-standing without connecting parts, for example, centrifuges. Further examples: vibratory screens, dynamic materials testing machines, and industrial processing vibrating machinery.

Examples for Evaluation Limits

The evaluation limits for machine groups K, M, G, and T can be taken from the following table.

For the machine groups D and S, no corresponding diagrams and limit values have been generated. In regard to these groups, we refer to the explicit explanations of the VDI Guideline 2056 (VDI-Verein Deutscher Ingenieure: Association of German Engineers).

Machine Group		Evaluation Levels (V_{rms} in mm/s)			
VDI	ISO	Good	Satisfactory	Still Acceptable	Unacceptable
K	I	< 0.7	0.7 ... 1.8	1.8 ... 4.5	> 4.5
M	II	< 1.1	1.1 ... 2.8	2.8 ... 7.1	> 7.1
G	III	< 1.8	1.8 ... 4.5	4.5 ... 11.0	> 11.0
T	IV	< 1.8	1.8 ... 18.0	18.0 ... 18.0	> 18.0

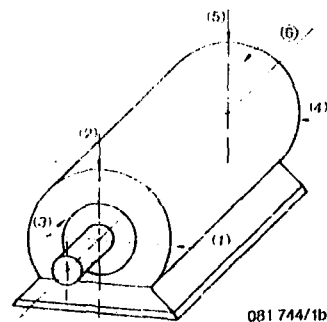
Table 2: Evaluation Limits according to VDI Guideline 2056 and ISO Standard 2373

NOTE:

Since these excerpts cannot replace the exact explanations of the above-mentioned standards, the user is urged to read these standards. They can be ordered from Beuth-Vertrieb GmbH, Burggrafenstraße 4–10, D-1000 Berlin 30.

6.1.5 Evaluation Criteria According to DIN 45665 and ISO 2373

DIN 45665 as well as the ISO Standard 2373 are based on the VDI Guidelines 2056 and ISO Standard 2372 respectively and are valid for the measuring and evaluation of the vibration severity at rotating electrical machinery of standard size with shaft heights between 80 and 315 mm. The machine should be operated with the rated voltage and nominal frequency (with alternating current) and the vibration measuring should be taken at nominal speed. If there are no other stipulations, the vibration severity measurement takes place in the no-load run and at a temperature which the machine has reached after having been in the no-load state for some time. The recommended measuring locations are shown in Fig. 5.



081 744/1b

Fig. 5: Measuring Locations

In Table 3, the admissible maximum values of the vibration **severity** for the different sizes are shown in the three vibration severity levels Normal (N), Reduced (R), and Special (S).

Evaluation level	Speed range	Limit values of the Vibration severity (V_{rms} ; SUM 10 ... 1000 Hz) for shaft heights		
		80 ... 132 mm	160 ... 225 mm	250 ... 315 mm
N (Normal)	600 ... 1800			
	1800 ... 3600	1.8 mm/s	2.8 mm/s	4.5 mm/s
R (Reduced)	600 ... 1800	0.71 mm/s	1.12 mm/s	1.8 mm/s
	1800 ... 3600	1.12 mm/s	1.8 mm/s	2.8 mm/s
S (Special)	600 ... 1800	0.45 mm/s	0.71 mm/s	1.12 mm/s
	1800 ... 3600	0.71 mm/s	1.12 mm/s	1.8 mm/s

Table 3: Recommended Limit Values according to DIN 45665 and ISO 2373 for Electrical Machinery.

NOTE:

Since these excerpts cannot replace the exact explanations of the above-mentioned standards, we recommend that they be read. The standards can be ordered from Beuth-Vertrieb GmbH, Burggrafenstraße 4 - 10, D-1000 Berlin 30.